Thermodynamic Stability of Nano-grained Alloys Against Grain Coarsening and Precipitation of Macroscopic Phases

GEORGE KAPTAY

Thermodynamic conditions are derived here for binary alloys to have their grain boundary (GB) energies negative, ensuring the stability of some nano-grained (NG) alloys. All binary alloys are found to belong to one of the following three types. Type 1 is the unstable NG alloy both against grain coarsening and precipitation of a macro-phase. Type 2 is the partly stable NG alloy, stable against coarsening but not against precipitation. Type 3 is the fully stable NG alloy, both against coarsening and precipitation. Alloys type 1 have negative, or low-positive interaction energies between the components. Alloys type 2 have medium-positive interaction energies, while alloys type 3 have high-positive interaction energies. Equations are derived for critical interaction energies separating alloys type 1 from type 2 and those from type 3, being functions of the molar excess GB energy of the solute, temperature (T) and composition of the alloy. The criterion to form a stable NG alloy is formulated through a new dimensionless number (Ng), defined as the ratio of the interaction energy to the excess molar GB energy of the solute, both taken at zero Kelvin. Systems with Ng number below 0.6 belong to alloy type 1, systems with Ng number between 0.6 and 1 belong to alloy type 2, while systems with Ng number above 1 belong to alloy type 3, at least at $T = 0$ K. The larger is the Ng number, the higher is the maximum T of stability of the NG alloy. By gradually increasing temperature alloys type 3 convert first into type 2 and further into type 1. The Ng number is used here to evaluate 16 binary tungsten-based (W-B) alloys. At $T = 0$ K type 3 NG alloys are formed with B = Cu, Ag, Mn, Ce, Y, Sc, Cr; type 2 is formed in the W-Ti system, while type 1 alloys are formed with B = Al, Ni, Co, Fe, Zr, Nb, Mo and Ta. For the W-Ag system the region of stability of the NG alloys is shown on a calculated phase diagram, indicating also the stable grain size.

https://doi.org/10.1007/s11661-019-05377-9

I. INTRODUCTION

NANO-MATERIALS play an increasing scientific and social role.[1–19] In the past, nano-materials were simplified to single nano-particles. However, it has been clear for some decades that the real use of nano-materials is expected if they form macroscopic articles with nano-structure inside. One class of such materials is the poly-crystalline nano-grained (NG) alloys. It should be admitted that producing such NG alloys is easier than to ensure their long-term stability, especially at high-temperatures when diffusion is fast enough to drive materials towards their equilibrium state within reasonable times.[20–28] That is why the purpose of this paper is to develop a model for thermodynamic stability of such NG alloys. Although there is plenty of previous literature on both the synthesis[29–47] and on modeling the stabilization of NG alloys[48–88]) (see also reviews[89–93]), the present paper is novel as it puts this question into a wider framework of the nano-Calphad method,[94,95] *i.e.*, into the thermodynamic framework originally developed by Gibbs.[96]

All previous models on GB stability apply the simplest Langmuir–McLean model[97,98] (see also Reference 99) for modeling grain boundary (GB) energy. Since the pioneering works of Weismuller[48,49] it is known that for the stabilization of PC-NG alloys strong repulsion between the components is needed in the bulk alloy. Thus, there is an inner contradiction in the previous sentences, as the original Langmuir model[97] treated the surface layer as an ideal solution, and so this modeling framework is not suited to describe strongly interacting systems. The novelty of the present paper is

GEORGE KAPTAY is with the Department of Nanotechnology, University of Miskolc, Miskolc, Egyetemvaros, 3515 Hungary, and also with the MTA-ME Materials Science Research Group, Miskolc, Egyetemvaros, 3515 Hungary, and also with the BAY-ENG Division, Bay Zoltan Applied Research Ltd, Miskolc, 2 Igloi, 3519, Hungary. Contact e-mail: kaptay@hotmail.com

Manuscript submitted March 31, 2019.

Published online: 06 August 2019

that here the extended Butler equation is applied to describe the GB energy.[100] As the Butler equation[101] was originally designed for strongly interacting systems, it provides a more natural framework to describe the stability of strongly interacting NG alloys.

The interplay between thermodynamic and kinetic reasons of the stability of NG alloys has been also discussed[102–106] (see also References 107 through 111). However, in the present paper only thermodynamic aspects will be discussed in a novel way.

II. ON THERMODYNAMIC INSTABILITY OF ONE-COMPONENT NG METALS

Following the original ideas of Gibbs,[96] the total absolute Gibbs energy of a one-component (A) NG metal (G°_{A}, J) can be written as:

$$G^{\circ}_{A} = G^{\circ}_{b,A} + A \cdot \sigma^{\circ}_{A} \quad [1]$$

where $G^{\circ}_{A,b}$ (J) is the bulk term of G°_{A} without grain boundaries, the latter being, the total Gibbs energy of a one-component (A) bulk single crystal, A (m^2) is the total interface area of grain boundaries within the poly-crystal, σ°_{A} (J/m^2) is the grain boundary (free) energy in a pure A crystal. Now, let us divide Eq. [1] by n°_{A} (mole), which is the amount of matter in the phase considered in Eq. [1][95]:

$$G^{\circ}_{m,A} = G^{\circ}_{m,b,A} + A_{sp} \cdot V^{\circ}_{m,A} \cdot \sigma^{\circ}_{A} \quad [2]$$

where $G^{\circ}_{m,A}$ (J/mol) is the molar Gibbs energy of a one-component NG metal, $G^{\circ}_{m,b,A}$ (J/mol) is the standard molar Gibbs energy of a one-component single crystal with no grain boundaries, $V^{\circ}_{m,A}$ (m^3/mol) is the molar volume of pure component A, A_{sp} (1/m) is the average specific interfacial area of the grain boundaries, defined as:

$$A_{sp} \equiv \frac{A}{V} \quad [3]$$

where V (m^3) is the total volume of the NG metal. The average specific interfacial area of 3-dimensional grains can be modeled as:

$$A_{sp} \cong \frac{k}{r} \quad [4]$$

where r (m) is the average effective grain radius, k (dimensionless) is the semi-empirical constant, depending on the shape of an average grain. For a spherical grain of radius r: $k = 3$, while for the cubic grain of the same *volume:* $k = 3.72$. However, in reality grains are polyhedral (see Figure 1), and for the polyhedral grains of the same volume as that of a sphere of radius r the following average value will be used in this model: $k \cong 3.36$. Substituting this latter value and Eq. [4] into Eq. [2], the final equation for the molar Gibbs energy of the NG metal follows as:

$$G^{\circ}_{m,A} \cong G^{\circ}_{m,b,A} + \frac{3.36}{r} \cdot V^{\circ}_{m,A} \cdot \sigma^{\circ}_{A} \quad [5]$$

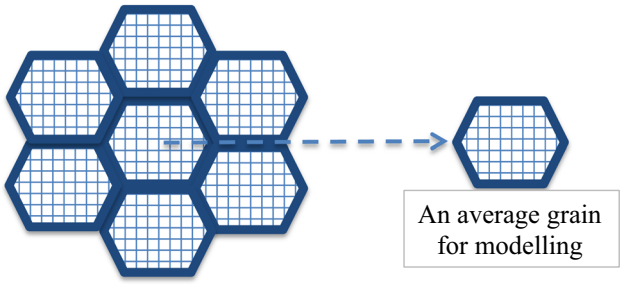

Fig. 1—Crystalline grains of polyhedral shapes are surrounded by amorphous grain boundaries marked by thick lines around the grains.

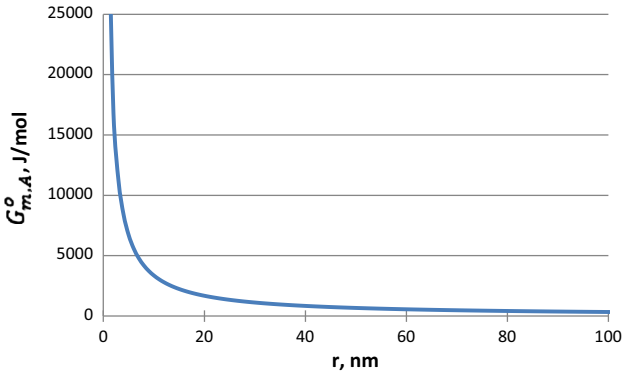

Fig. 2—The molar Gibbs energy of a one-component NG metal as function of the average radius of its grains calculated by Eqs. [5] and [6] and parameters from Table I.

In bulk thermodynamics, the standard Gibbs energy of pure component A at any temperature is usually taken by definition and for simplicity equal zero, as a reference value:

$$G^{\circ}_{m,b,A} \equiv 0 \quad [6]$$

Equation [5] is shown graphically in Figure 2 taking into account Eq. [6] with parameters of Table I. One can see that the molar Gibbs energy of a NG one-component metal gradually decreases with increasing the grain size from a high-positive value towards the zero value written by Eq. [6], the latter being valid for a macroscopic single crystal. Thus, it follows that a one-component NG metal can never be more stable thermodynamically than the macroscopic single crystal. This is because all values in the second term of Eq. [5] can have only positive values for one-component metals, including the GB energy.

Similar to pure metals, the specific surface area and the molar volume have always positive values even for alloys. However, contrary to pure metals, the GB energy can be also negative for alloys under special conditions.[48] If this is indeed the case, then NG alloys of special compositions can be more stable compared to the corresponding bulk single crystals, at least in a

limited temperature range. In the next sections, the thermodynamic conditions of the stability of NG alloys will be discussed.

III. SELECTION OF MODELS AND PARAMETERS TO DEMONSTRATE THE STABILITY OF NG ALLOYS

In the present paper, the essential conditions for the thermodynamic stability of NG alloys are demonstrated. For this purpose, the simplest possible set of models and model parameters will be applied, necessary for stabilization. All those details will be neglected which are not necessarily needed for this demonstration. All those neglected details would provide only small quantitative changes for the final result, without any qualitative influence. Parameter values for demonstrational purposes are given in Table I.

As was shown above, stability is not possible for one-component metals. The minimum requirement to ensure stable NG alloys is to have a two-component alloy, so this is our choice here. Let us mention that if the number of components in the alloy is increased further, the configurational entropy of the macro-solid solution will increase, stabilizing the macro-alloy *vs* the NG alloy (see the extra-stability of high-entropy macro-alloys). Thus, multi-component alloys are not preferred *vs* binary alloys to stabilize NG alloys.

The poly-crystalline alloy modeled here is not limited in its total size, thus it contains virtually an infinite number of nano-grains. However, for modeling purposes each nano-grain is considered equal. In real life, it means that we consider an average nano-grain with average properties. An average nano-grain will be characterized by its effective radius (r, m) of its bulk not including the thickness of the GB surrounding this grain. The volume of the grain is calculated as if the grain was spherical, but its surface area is calculated by Eqs. [3] and [4] with the average value of $k = 3.36$ (see above).

For simplicity, we suppose that the two solid components A and B of the binary system have in equilibrium the same crystal structure, and Eq. [6] is valid for both of them. We also presume for simplicity that the thermodynamics of the solid solution between components A and B can be described by the simplest regular solution model. However, the exponential T-dependence of the interaction energy will be taken into account below; in this way, implicitly the excess molar entropy is taken into account. We take this T-dependence into account, as it has a much more significant influence on the maximum stability of the NG alloys compared to the neglected T-dependence of $\omega_B^\circ \cdot \sigma_B^\circ$ (see below).

Table I. Simplified Parameters Used for Model Calculations

Quantity	Unit	Value	Source
$G_{m,b,A}^\circ$	J/mol	0	Eq. [6]
$G_{m,b,B}^\circ$	J/mol	0	Eq. [6]
σ_A°	J/m^2	1.00	arbitrary
σ_B°	J/m^2	0.30	$\sigma_B^\circ < \sigma_A^\circ$
$V_{m,A}^\circ$	cm^3/mol	10.0	arbitrary
$V_{m,B}^\circ = V_{m,L,B}^\circ$	cm^3/mol	15.0	arbitrary
β	—	0.90	approximated
f	—	1.25	for bcc grains
ω_A°	m^2/mol	4.90 10^4	Eq. [8a]
ω_B°	m^2/mol	6.42 10^4	Eq. [8b]
r_a	nm	0.157	Eq. [19]
r_{min}	nm	4.3	Eq. [23a]

It is also presumed here for simplicity that although the pure components A and B have different molar volumes (denoted as $V_{m,A}^\circ$ and $V_{m,B}^\circ$, both in m^3/mol), their temperature dependence has a negligible effect on the stability of NG alloys. Note that in Table I, the ratio $V_{m,B}^\circ/V_{m,A}^\circ = 1.5$ is selected, as it is in the middle of the interval of actual systems considered in Table II with values of $V_{m,B}^\circ/V_{m,A}^\circ$ ranging from 0.7 to 2. In addition, we will suppose for simplicity that the molar volume of the A–B solid solution will be a linear combination of $V_{m,A}^\circ$ and $V_{m,B}^\circ$ along the mole fraction of component B, *i.e.*, the excess molar volume of the alloy is also neglected for simplicity. For simplicity, it is also supposed that the molar volume of pure solid and pure liquid B is the same: $V_{m,B}^\circ = V_{m,L,B}^\circ$.

We also presume for simplicity that although the pure components A and B have different GB energies, their temperature dependence and their orientation dependence are neglected. Thus, for simplicity only high-angle GBs are taken into account, with an average GB (free) energy, denoted as σ_A° and σ_B° (both in J/m^2). Other (low angle) GBs are neglected for simplicity, as they have smaller GB energies. In addition, the outer surface area of the alloy is neglected as it is usually much smaller compared to the total GB interfacial area within the NG alloy; moreover, its contribution is identical for the NG alloy and for the reference macro-alloy, so this term falls out when the two are compared. However, the GB energy of the alloy will be not a linear combination of σ_A° and σ_B° along the average mole fraction of the alloy, as preferential segregation of the component with smaller GB energy will be considered. Component B will be selected as the GB-active component, so in this paper: $\sigma_A^\circ > \sigma_B^\circ$.

Three state parameters will be considered in this paper: the average mole fraction of component B in the alloy (denoted by x, dimensionless), absolute temperature (T, K) and the average radius of the bulk of the grain (r, m). The radius of the grain is an independent state parameter here as the concentration and temperature dependences of the molar volumes of the components are neglected. Pressure will be kept at standard constant value of 1 bar. As condensed phases are studied here, all results will be identical below 100 bar.

This paper is written using mostly the methods of chemical thermodynamics, which is a statistical science. Therefore, care will be taken to make sure that there are at least 1000 atoms in each nano-grain. Taking into account the average molar volume of 10 cm^3/mol of metals and supposing for simplicity that the grains are spherical, the effective radius of each nano-grain studied in this paper will be larger than $r = 1.6$ nm. Therefore,

the results of the present paper will be valid for NG alloys with average grain diameters above 3.2 nm.

IV. A MODEL FOR THE CONCENTRATION DEPENDENCE OF THE GB ENERGY

In this paper, the GB energy will be modeled using the extended Butler model.[100] The original Butler model was developed for surface tension of a liquid/gas surface[101] and it was criticized in the literature for using un-defined partial surface tensions of the components and for being not consistent with thermodynamics of Gibbs. Recently, the partial surface tensions of the components were defined[112] in agreement with the thermodynamics of Gibbs and it was proven that even in this case the original Butler equations follow. Additionally, it was proven that the Butler equations can also be derived from the requirement that a solution phase should have a minimum Gibbs energy including its surface term.[113] This question was reviewed recently.[95]

In this section, the GB energy will be modeled without size restrictions, *i.e.*, the bulk and average mole fractions will be taken as identical (denoted as x for the average mole fraction of component B). It will be supposed, however, that the mole fraction of component B in the GB will have a different value, denoted as x_{gb}. Then, the two partial GB energies of the two components are written as[100]:

$$\sigma_A = \sigma_A^\circ + \frac{R\cdot T}{\omega_A^\circ}\cdot \ln\left(\frac{1-x_{gb}}{1-x}\right) + \frac{\Omega}{\omega_A^\circ}\cdot\left(\beta\cdot x_{gb}^2 - x^2\right) \quad [7a]$$

$$\sigma_B = \sigma_B^\circ + \frac{R\cdot T}{\omega_B^\circ}\cdot \ln\left(\frac{x_{gb}}{x}\right) + \frac{\Omega}{\omega_B^\circ}\cdot\left[\beta\cdot\left(1-x_{gb}\right)^2 - (1-x)^2\right] \quad [7b]$$

where σ_A and σ_B (J/m^2) are the partial GB energies of components A and B, respectively, σ_A^o and σ_B^o (J/m^2) are the GB energies of pure components A and B, respectively, R = 8.3145 J/molK is the universal gas constant, T (K) is the absolute temperature, Ω (J/mol) is the bulk interaction energy between components A and B in the framework of the regular solution model, β is the ratio of bonds in the GB to the same in the bulk of the grain, ω_A° and ω_B° (m^2/mol) are the molar GB areas of the pure components A and B, respectively, written after Skapski as[114]:

$$\omega_A^\circ = f\cdot\left(V_{m,A}^\circ\right)^{2/3}\cdot N_{Av}^{1/3} \quad [8a]$$

$$\omega_B^\circ = f\cdot\left(V_{m,B}^\circ\right)^{2/3}\cdot N_{Av}^{1/3} \quad [8b]$$

where f (dimensionless) is a geometric parameter, N_{Av} = 6.02 10^{23} 1/mol is the Avogadro number. Equations ([7a], [7b]) are two versions for the two components of the first extended Butler equation. The second extended Butler equation states that the GB energy of the alloy (= solid solution) and the partial GB energies of the components of the same solid solution must be equal in equilibrium[100,101]:

$$\sigma = \sigma_A = \sigma_B \quad [9]$$

To perform calculations with Eqs. [7] through [9] the following initial information must be known for the given A–B system: σ_A°, $V_{m,A}^\circ$, σ_B°, $V_{m,B}^\circ$, Ω. Additionally, the model parameters β and f should be known. Finally, the state parameters should be given: x and T (note: p = 1 bar is fixed above for the whole paper). If the values of all these parameters are given, then, first Eqs. [7a] and [7b] should be substituted into the right-hand side of Eq. [9] ($\sigma_A = \sigma_B$) and from here the equilibrium mole fraction of component B in the GB region is found (x_{gb}). Then, substituting this latter value back into Eqs. [7a] and [7b], both σ_A and σ_B are calculated. These two later values must be equal, and according to Eq. [9] their values also equal the GB energy of the alloy (= solid solution).

Now, let us estimate the model parameters. Parameter β will fall out later, so it is sufficient to provide here only its approximated value: $\beta \cong 0.90$. Parameter f follows from geometrical considerations[115]:

$$f = \left(\frac{3\cdot f_b}{4}\right)^{2/3}\cdot\frac{\pi^{1/3}}{f_{gb}} \quad [10]$$

where f_b (dimensionless) is the 3-dimensional bulk packing fraction within the grain, f_{gb} (dimensionless) is the 2-dimensional packing fraction along the GB if one looks perpendicular at the GB. Now, let us assume that the bulk packing fractions of the bulk grains are the same as in macroscopic crystals, *i.e.*, f_b = 0.74 for an fcc grain and f_b = 0.68 for a bcc grain. The GB is assumed to be in a liquid-like amorphous state, with a 3-dimensional packing fraction of about 0.65.[115] Thus, the 2-dimensional packing fraction is about $f_{gb} \cong 0.65^{2/3} = 0.75$. Substituting these values into Eq. [10]: $f \cong 1.32$ for an fcc grain and $f \cong 1.25$ for a bcc grain.

Now, let us perform a calculation using the model parameters of Table I at state parameter values of x = 0.15 and T = 500 K. The equilibrium values for both x_{gb} and σ as function of the bulk interaction energy (Ω) are plotted in Figure 3. As follows from Figure 3(b), the GB energy becomes negative above a certain interaction energy value. As follows from Figure 3(a), around this value the GB is made almost exclusively of component B: $x_{gb} \cong 1$. Substituting this value into Eqs. [7b] and [9], the following approximated equation is obtained:

$$\sigma \cong \sigma_B^\circ - \frac{R\cdot T}{\omega_B^\circ}\cdot\ln x - \frac{\Omega}{\omega_B^\circ}\cdot(1-x)^2 \quad (\text{at } x_{gb}\cong 1) \quad [11a]$$

Substituting into Eq. [11a] the parameter values from Table I and those given above, the following simplified equation is obtained (in J/m^2 and kJ/mol):

$$\sigma \cong 0.423 - 1.13 \cdot 10^{-5} \cdot \Omega \qquad [11b]$$

The broken line calculated by Eq. [11b] in Figure 3(b) overlaps the results of the numerical calculations in the whole region with $x_{gb} \cong 1$. The special value Ω_{gb} can be expressed from Eq. [11a] at which $\sigma = 0$ (and at $\Omega > \Omega_{gb} : \sigma < 0$):

$$\Omega_{gb} \cong \frac{\omega_B^\circ \cdot \sigma_B^\circ - R \cdot T \cdot \ln x}{(1-x)^2}. \qquad [12]$$

Substituting the values from above and from Table I into Eq. [12]: $\Omega_{gb} \cong 37.6$ kJ/mol, which is in agreement with Figure 3(b). As follows from Eq. [12], at $x = 0$ and $x = 1$: $\Omega_{gb} = \infty$. As this is an unrealistic requirement, for pure metals $\sigma \leq 0$ is indeed impossible.

As follows from Figure 3(b) and Eq. [12], the GB energy will be negative when the interaction energy has a large-positive value. However, in this case, the bulk solid A-B solution tends to separate into the mixture of two solid solutions of different compositions. The critical value of the interaction energy when such phase separation takes place is expressed from the theory of regular solution model as:

$$\Omega_{cr} = \frac{R \cdot T}{2 \cdot x - 1} \cdot \ln\left(\frac{x}{1-x}\right) \quad (\text{for } x \neq 0.5) \qquad [13]$$

Substituting parameters $x = 0.15$ and $T = 500$ K into Eq. [13]: $\Omega_{cr} = 10.3$ kJ/mol. Compared to the above value of $\Omega_{gb} \cong 37.6$ kJ/mol it follows that $\Omega_{cr} < \Omega_{gb}$ (see also Figure 3(b)). It can be generally proven that this inequality is obeyed at any reasonable values of $\omega_B^\circ \cdot \sigma_B^\circ$, x and T.[116] It means that when the A–B system is in equilibrium as a 1-phase macroscopic solid solution, then $\sigma > 0$, which is a usual boundary condition for any interfacial energy. On the other hand, $\sigma < 0$ takes place only, when the A–B system is in equilibrium as a mixture of two macroscopic solutions of different compositions; however, in this case the Butler equation is not valid as applied above, thus $\sigma < 0$ is not a real result for macroscopic equilibrium systems. On the other hand, for nanograins, the mutual solubility of the components is increased,[117] thus for NG alloys the case of $\sigma < 0$ is possible also in equilibrium (see below).

Equation [11a] is one of the most essential equations of this paper. Let us note that in the literature different equations are published instead of Eq. [11a]. However, their detailed critical analysis goes out of the framework of the present paper.

V. THE MODEL FOR THE MOLAR GIBBS ENERGY OF MACROSCOPIC ALLOYS

Now, let us select two metallic components A and B with the same equilibrium crystal structure from 0 K till their melting points. Suppose that Eq. [6] will be valid for both solid components, so the molar Gibbs energy of the mechanical mixture of the two pure solid components will

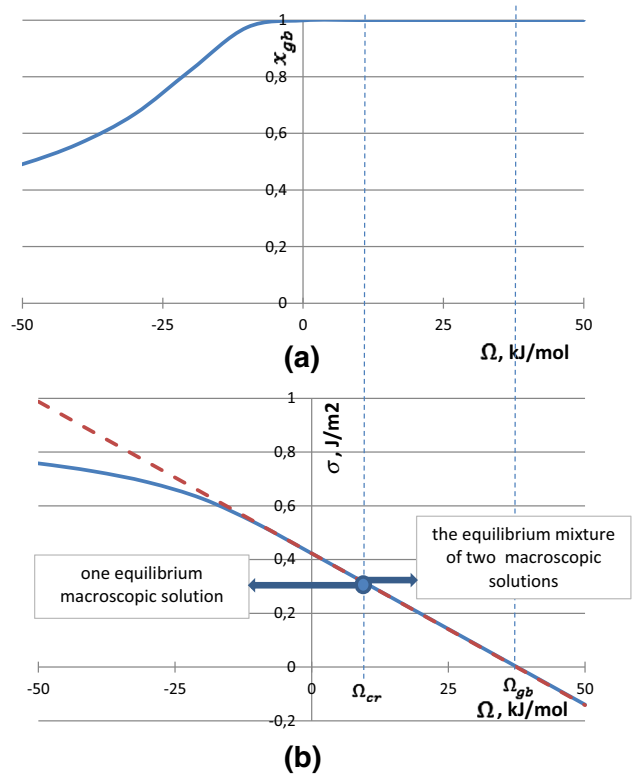

Fig. 3—The equilibrium mole fraction of component B in the GB (*a*) and the equilibrium GB energy (*b*) as function of interaction energy (Ω) calculated by Eqs. [7] through [9], using parameters of Table I with $x = 0.15$ and $T = 500$ K. The dotted line is calculated by Eq. [11b]. The vertical thin-dotted lines correspond to Ω_{gb} and Ω_{cr} calculated by Eqs. [12] and [13].

be zero at any temperature. For the solid A–B-solution the simplest regular solution model will be applied with a temperature-independent interaction energy parameter Ω, having a high-positive value to ensure negative grain boundary energy and thus the stabilization of the NG alloy (see above). Thus, the equilibrium state for the macroscopic alloy will be the mixture of two solid solutions, with equilibrium mole fractions of component B in the two solutions denoted as x_e and $1 - x_e$. Let us note that the average mole fraction of component B in the alloy should be in the interval between these two values. The molar Gibbs energy of this equilibrium mixture of two solid solutions will be calculated as:

$$G_{m,mac} = R \cdot T \cdot [x_e \cdot \ln x_e + (1 - x_e) \cdot \ln(1 - x_e)] + \Omega \cdot x_e \cdot (1 - x_e) \qquad [14]$$

To find the equilibrium value of x_e, the minimum point of $G_{m,mac}$ as function of x_e should be found from Eq. [14]. For that the first derivative of $G_{m,mac}$ is taken by x_e and then this expression is made equal 0. There are three solutions to this latter equation. The one with the smallest x_e value is of interest for us. Unfortunately, the resulting equation does not have an analytical solution, so the numerical solution is found for the smallest possible value of x_e of the following equation:

$$R \cdot T \cdot \ln\left(\frac{x_e}{1-x_e}\right) + \Omega \cdot (1 - 2 \cdot x_e) = 0 \qquad [15a]$$

For example, at $T = 500$ K and $\Omega = 50$ kJ/mol the solution of Eq. [15a] is: $x_e \cong 5.9803 \cdot 10^{-6}$. One can see that this value is negligible compared to 1 or even to 0.5. Therefore, the following approximated solution of Eq. [15a] can be found if $1 - 2 \cdot x_e \cong 1$ is supposed:

$$x_e \cong \exp\left[-\frac{\Omega}{R \cdot T}\right] \qquad [15b]$$

Substituting the above values of $T = 500$ K and $\Omega = 50$ kJ/mol into Eq. [15b]: $x_e \cong 5.9795 \cdot 10^{-6}$ is obtained. When the two above solutions to Eqs. [15a] and [15b] are substituted into Eq. [14], the two results are: $G_{m,mac} = -0.0249$ and -0.0254 J/mol, the difference being below 0.001 J/mol. This difference is insignificant, so Eqs. [14] and [15b] can be used in the first approximation to calculate the reference value of the molar Gibbs energy.

The NG alloy will be thermodynamically fully stable, if the minimum value of its molar Gibbs energy *vs* its radius will be more negative than the reference value calculated by Eqs. [14] and [15b]. This reference value will be valid at any temperature below the eutectic temperature of the eutectic type and eutectic + monotectic type phase diagrams. On the other hand, the same will be valid at any temperature below the melting point of the lower melting component for the peritectic type and the peritectic + monotectic type phase diagrams.

VI. THE MATERIAL BALANCE FOR NG ALLOYS

The material balance should be separately discussed as an average grain shown in Figure 1 should be divided into its crystalline bulk and into its amorphous half-GB. All physical parameters will be denoted by subscript "b" for the bulk of the grain and by subscript "gb" for the half-GB (note: any GB belongs to two grains, so a half-GB belongs to each grain). For example, the average mole fraction of component B in the alloy and in the average grain (denoted as x) will be divided into a value x_b (defined as the mole fraction of component B in the bulk of the grain) and x_{gb} (defined as the mole fraction of component B in the GB). For the case when the NG alloys are expected to be stable, *i.e.*, the GB energy is expected to have a negative value, the approximation of $x_{gb} \cong 1$ is valid (see Figure 3(a)), *i.e.*, the GB is composed almost entirely of component B, due to its segregation to the GB (and due to the selection made above: $\sigma^\circ_A > \sigma^\circ_B$).

Now, let us denote the average effective radius of the bulk of the grain as r (m). As was explained above, the volume of the bulk of the grain is modeled as that of a sphere:

$$V_b = 4.189 \cdot r^3 \qquad [16]$$

The amount of matter within the bulk of the grain can be found as the ratio of its volume to its molar volume:

$$n_b = \frac{V_b}{V_{m,b}} \qquad [17]$$

where $V_{m,b}$ (m^3/mol) is the molar volume of the bulk of the grain, which can be calculated as the linear combination of the molar volumes of the pure components as function of the bulk mole fraction of component B:

$$V_{m,b} = V^\circ_{m,A} + x_b \cdot \left(V^\circ_{m,B} - V^\circ_{m,A}\right) \qquad [18]$$

The radius of atom B in the GB region is expressed from the usual model for the molar volume of pure liquid B, supposing spherical atoms of radius r_a and the 3-D packing fraction of the grain boundary (0.65) as:

$$r_a = 0.5374 \cdot \left(\frac{V^\circ_{m,L,B}}{N_{Av}}\right)^{1/3} \qquad [19]$$

where $V^\circ_{m,L,B}$ (m^3/mol) is the molar volume of the pure liquid metal B. Substituting $V^\circ_{m,L,B} = 15$ cm^3/mol into Eq. [19]: $r_a = 0.157$ nm. As the GB is composed mostly of component B, the amount of matter in the half-GB is the same as the amount of component B in the same half-GB: $n_{gb} = n_{B,gb}$. This can be found as the number of B atoms in the half-GB divided by the Avogadro number. The number of B atoms in the half-GB follows as the surface area along the grain of radius $(r + r_a)$, increased by the shape factor of 3.36 / 3 = 1.12 (see above), multiplied by the 2-D packing fraction in the grain boundary region ($0.65^{2/3} = 0.75$, see above) and divided by the cross-sectional area of one atom ($= \pi \cdot r_a^2$). Then, the amount of matter in the half-GB is written as:

$$n_{gb} = n_{B,gb} = \frac{3.36}{N_{Av}} \cdot \frac{(r + r_a)^2}{r_a^2} \qquad [20]$$

By writing Eq. [20], it was supposed that the thickness of the half-GB is approximately a diameter of one B atom. According to the material balance, the average mole fraction of component B in the alloy multiplied by the total amount of matter in the grain must equal the sum of the amount of matter of component B in the bulk of the grain and the same in the half-GB. This condition can be written using Eqs. [16] through [20] as:

$$x \cdot \left[\frac{4.189 \cdot r^3}{V^\circ_{m,A} + x_b \cdot \left(V^\circ_{m,B} - V^\circ_{m,A}\right)} + \frac{3.36}{N_{Av} \cdot r_a^2} \cdot (r + r_a)^2\right] = x_b \cdot \frac{4.189 \cdot r^3}{V^\circ_{m,A} + x_b \cdot \left(V^\circ_{m,B} - V^\circ_{m,A}\right)} + \frac{3.36}{N_{Av} \cdot r_a^2} \cdot (r + r_a)^2 \qquad [21]$$

The bulk mole fraction of component B is expressed from Eq. [21], as:

$$x_b = \frac{4.189 \cdot x \cdot N_{Av} \cdot r_a^2 \cdot r^3 - 3.36 \cdot (1-x) \cdot V^\circ_{m,A} \cdot (r + r_a)^2}{4.189 \cdot N_{Av} \cdot r_a^2 \cdot r^3 + 3.36 \cdot (1-x) \cdot \left(V^\circ_{m,B} - V^\circ_{m,A}\right) \cdot (r + r_a)^2} \quad [22]$$

The boundary condition following from Eq. [22] is reasonable: at r approaching infinity x_b approaches the value of x. That is why no difference was made between the bulk mole fraction and the average mole fraction in Section IV. On the other hand, Eq. [22] can lead to $x_b = 0$, if the size of the grain has its minimum possible value (r_{min}); this condition can be expressed from Eq. [22] as:

$$1.247 \cdot x \cdot N_{Av} \cdot r_a^2 \cdot r_{min}^3 = (1-x) \cdot V^\circ_{m,A} \cdot (r_{min} + r_a)^2 \quad [23a]$$

When $r_{min} \gg r_a$, Eq. [23a] has the following simple analytical solution:

$$r_{min} \cong 0.802 \cdot \frac{(1-x)}{x} \cdot \frac{V^\circ_{m,A}}{N_{Av} \cdot r_a^2} \quad [23b]$$

where r_{min} (m) is the minimum size of the grain ($r > r_{min}$) that ensures the GB is fully covered by component B, *i.e.*, it ensures the possibility of the negative grain boundary energy, thus the stability of the NG alloy. Substituting the parameter values of $V^\circ_{m,A} = 10\,cm^3/mol$, $x = 0.15$ and $r_a = 0.157\,nm$ into Eq. [23b], the result of this approximated equation is: $r_{min} = 3.1$ nm, while the numerical solution of the exact Eq. [23a] provides the value of $r_{min} = 3.4$ nm. The dependence of r_{min} on x is shown in Figure 4. As will be shown below, the equilibrium grain radius (r_{eq}, m) is only slightly larger than the value of r_{min}, thus Eq. [23b] and Figure 4 can serve as a design equation and a design graph for the equilibrium grain size of the NG alloys in a first approximation.

As follows from Figure 4, to stabilize smaller grain size, higher average concentration of component B is needed. Let us note that this latter conclusion has been known since the work of Weismuller.[48] Eq. [23b] can also be used to express the minimum average mole fraction of component B, needed to stabilize the grain of radius r:

$$x_{min} \cong \frac{0.802 \cdot V^\circ_{m,A} \Big/ N_{Av} \cdot r_a^2}{r + 0.802 \cdot V^\circ_{m,A} \Big/ N_{Av} \cdot r_a^2} \quad [24]$$

Substituting the above parameters and r = 1.6 nm into Eq. [24], the value of $x_{min} \cong 0.25$ is found. From the numerical solution of Eq. [23a] $x_{min} \cong 0.29$ is found. Thus, the present model will be thermodynamically valid below about $x = 0.3$ (see also Figure 7(b) below).

VII. THE MOLAR GIBBS ENERGY OF NG ALLOYS; DEMONSTRATION OF THE THREE ALLOY TYPES

The molar Gibbs energy of the NG alloy ($G_{m,nano}$, J/mol) can be written in an analogous way with Eq. [5] as:

$$G_{m,nano} \cong G_{m,nano,b} + \frac{3.36}{r + 2 \cdot r_a} \cdot V_{m,b} \cdot \sigma \quad [25]$$

where $G_{m,nano,b}$ (J/mol) is the bulk molar Gibbs energy of the NG alloy written by Eq. [26], while σ (J/m^2) is the grain boundary energy of the alloy, written by Eq. [27]:

$$G_{m,nano,b} = R \cdot T \cdot [x_b \cdot \ln x_b + (1-x_b) \cdot \ln(1-x_b)] + \Omega \cdot x_b \cdot (1-x_b) \quad [26]$$

$$\sigma \cong \sigma^\circ_B - \frac{R \cdot T}{\omega^\circ_B} \cdot \ln x_b - \frac{\Omega}{\omega^\circ_B} \cdot (1-x_b)^2 \quad [27]$$

Note that Eq. [26] is similar to Eq. [14] with x_e replaced by x_b, while Eq. [27] is similar to Eq. [11a] with x replaced by x_b. In both Eqs. [26] and [27] x_b is calculated by Eq. [22]. In the second term of Eq. [25] the outer radius of the grain ($r + 2 \cdot r_a$) is used instead of r, as the latter is only the radius of the bulk of the grain, while the former is the radius of the whole grain including the double thickness of the half-GB.

The calculation is performed using parameters of Table I with $x = 0.12$ and $T = 500$ K. From here, $r_{min} = 4.3$ nm follows from Eq. [23a]. Therefore, the molar Gibbs energy will be calculated at $r \geq 4.3$ nm. The selected parameters should be substituted into Eq. [22] to calculate x_b. Then, all parameters, including this one should be substituted into Eqs. [25] through [27] to calculate the molar Gibbs energy of the NG alloy. The reference value $G_{m,mac}$ is calculated by Eqs. [14] and [15b]. The results of calculation are shown in

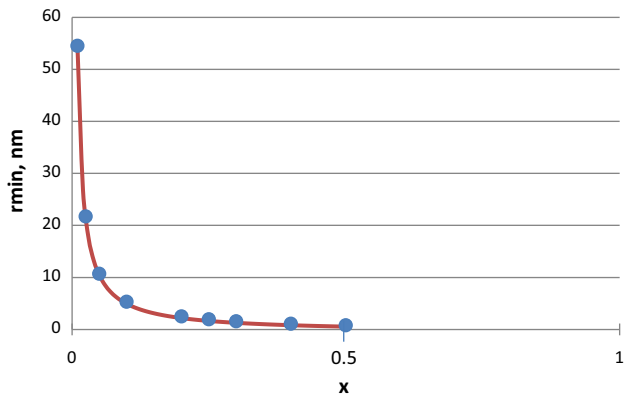

Fig. 4—The x-dependence of r_{min} calculated by Eq. [23b] (line) and obtained by numerical solution of Eq. [23a] (points), using parameters: $V^\circ_{m,A} = 10$ cm^3/mol, $x = 0.15$, $r_a = 0.157$ nm.

Figures 5(a) through (c), for three different values of the interaction energy Ω, corresponding to the following three types of NG alloys:

Type 1 NG alloy (with $\Omega = 20$ kJ/mol as an example in Figure 5(a)) is unstable both against grain coarsening and precipitation of a macro-phase; its molar Gibbs energy does not pass through a minimum as function of grain size and it is more positive at any grain size than that of the corresponding macro-alloy.
Type 2 NG alloy (with $\Omega = 35$ kJ/mol as an example in Figure 5(b)) is partly stable: it is stable against grain coarsening, but not against precipitation of a macro-phase; its molar Gibbs energy passes through a minimum as function of grain size, but the minimum molar Gibbs energy of the NG alloy is more positive than that of the corresponding macro-alloy at any grain size.
Type 3 NG alloy (with $\Omega = 50$ kJ/mol as an example in Figure 5(c)) is fully stable both against grain coarsening and precipitation of a macro-phase; its molar Gibbs energy passes through a minimum as function of grain size, and the minimum molar Gibbs energy of the NG alloy is more negative than that of the corresponding macro-alloy. In Figure 5(c) the equilibrium grain radius corresponding to this minimum point is: $r_{eq} = 4.6$ nm, being slightly larger than the value of $r_{min} = 4.3$ nm found above.

The evolution of the stability of NG alloys with increasing values of the interaction energy is similar to Figures 5(a) through (c) even if different parameter combinations are applied. Thus, type 1 alloys appear with interaction energies having negative or zero or low-positive values, type 2 alloys appear with interaction energies having medium-positive values, while type 3 alloys appear with interaction energies having large-positive values.

VIII. ON A STABILITY CRITERION AND STABILITY DIAGRAMS TO SELECT STABLE NG ALLOYS

As was shown above, even in the framework of the simplest model, the stability of NG alloys depends on seven independent parameters ($V^{\circ}_{m,A}$, $V^{\circ}_{m,B}$, σ°_{A}, σ°_{B}, Ω, T, x). If a more complex solution model, or the excess volume or the T-dependence of physical quantities are taken into account, the number of parameters can be easily doubled, at least (see for example the 24 parameters below for the real W-Ag system). Thus, the identification of a single stability criterion or at least a 2-dimensional stability graph seems elusive. Nevertheless, for fast screening of stable NG systems such a criterion or diagram is desirable.

Now, let us find such a simplified criterion for fully stable NG alloys (type 3). For this purpose, let us remind that the key to the full stability of NG alloys is the negative grain boundary energy. The minimum value of the interaction energy to reach this goal is written by

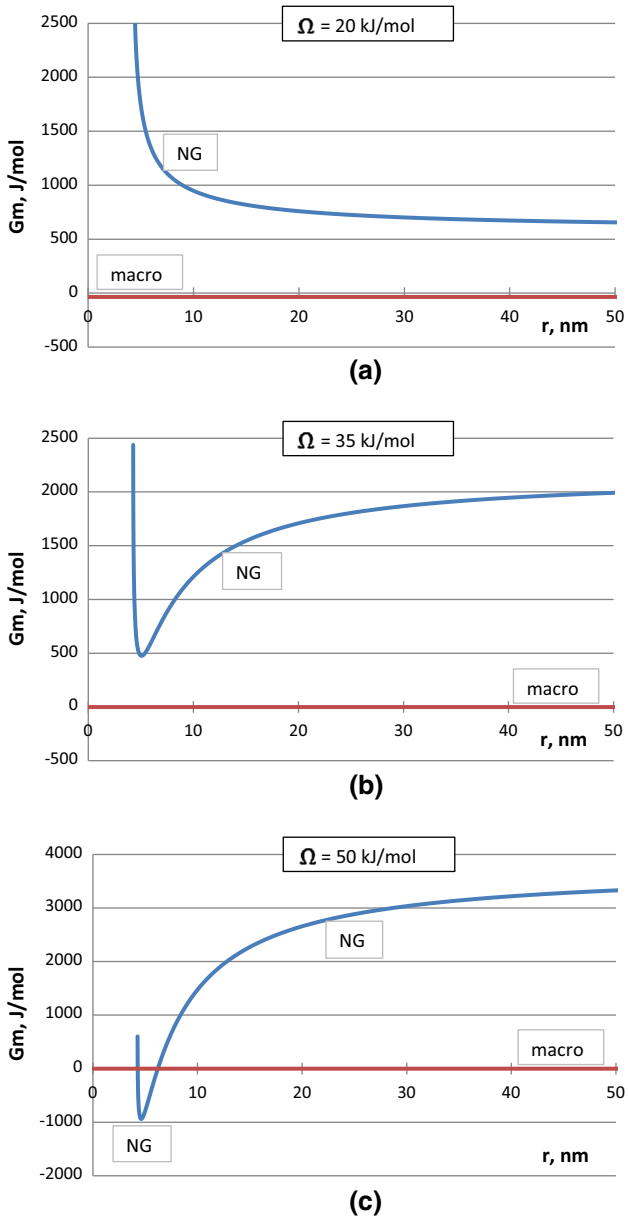

Fig. 5—The molar Gibbs energy of the NG alloy and that of the macro-alloy as function of the grain radius calculated by Eqs. [14], [15b], [22], [25] through [27] for $\Omega = 20$ kJ/mol (*a*), $\Omega = 35$ kJ/mol (*b*) and $\Omega = 50$ kJ/mol (*c*). Parameters are from Table I at $x = 0.12$ and $T = 500$ K.

Eq. [12]. Although this equation is relatively simple, it still contains 4 parameters on the right-hand side: ω°_{B}, σ°_{B}, T and x. It should be understood that the highest chance for the stability of NG alloys exists at $T = 0$ K. Partly because the value of Ω_{gb} increases with increasing temperature according to Eq. [12], and partly because the relative stability of macro-alloys also increases with temperature according to Eqs. [14] and [15b]. Thus, the minimum value of the interaction energy needed for stabilization of NG alloys can be found at $T = 0$ K.

Therefore, neglecting also the minor role of composition in Eq. [12], the following dimensionless number is introduced in this paper:

$$Ng \equiv \left(\frac{\Omega}{\omega_B^\circ \cdot \sigma_B^\circ}\right)_{0K} \qquad [28]$$

where the letters "Ng" stand for "Nano-grained" and the dimensionless Ng number is called here the "Ng number" or the "NG-alloy-stability number" or the "poly-crystalline nano-grained alloy stability number" and is defined as the ratio of the interaction energy between the components in the bulk A–B system to the excess molar GB energy of the GB-active solute, extrapolated to zero Kelvin. The major property of this new dimensionless number is that for A–B systems with $Ng \leq 1$ the given A–B system will not be fully thermodynamically stable as NG alloy at any temperature and at any composition. On the other hand, if $Ng > 1$, then the given A–B system will be fully stable as NG alloy at least in a limited temperature and composition range. The higher is the value of the Ng number (above 1) for the given A–B system the wider is the temperature-composition stability range of the given A–B system as NG alloy. Thus, the value of the Ng number can be used as a simple and fast criterion to select potentially stable NG systems. This is demonstrated for 16 W-based systems in Table II.

Looking at Eq. [12], the effect of temperature and composition can be taken into account using the following new complex, but single parameter Z, defined as:

$$Z \equiv -\frac{R \cdot T \cdot \ln x}{(1-x)^2} \cdot \quad \text{with } x < 0.5 \qquad [29]$$

where Z (J/mol) is an additional parameter having an influence on the stability of NG alloys. When $Z = 0$, the single Ng number is sufficient to predict whether the given A–B system is fully stable as NG alloy at least at 0 K. However, for different values of parameter Z, different demarcation lines will separate the fully stable / partly stable regions of the stability graph plotted in coordinates of Ω *vs* $\omega_B^\circ \cdot \sigma_B^\circ$ (both values taken at zero Kelvin). The following approximated equation is found here to predict the minimum interaction energy needed to fully stabilize the NG alloys:

$$\Omega_{stab} \geq \exp\left(\frac{Z}{66}\right) \cdot \left[1.40 \cdot Z + \omega_B^\circ \cdot \sigma_B^\circ \cdot \left(1 + 0.0235 \cdot Z^{0.715}\right)\right] \qquad [30]$$

where all physical quantities are substituted and obtained in kJ/mol. The parameters in the [ ] parenthesis of Eq. [30] are obtained by calculating the molar Gibbs energy of the NG alloys by Eqs. [22], [25] through [27] using a large variety of parameter combinations Ω (at $T = 0$ K) and $\omega_B^\circ \cdot \sigma_B^\circ$ (at $T = 0$ K), coupled with different values of parameter Z (using a variety of x and T combinations). For this procedure, the average molar volumes $V_{m,A}^\circ = 10$ cm^3/mol, $V_{m,B}^\circ = 15$ cm^3/mol are used and a bcc structure for the bulk of the grain is taken. Based on the above, the smallest possible values of $\Omega = \Omega_{stab}$ are searched that just ensure full stability of the NG alloys as function of $\omega_B^\circ \cdot \sigma_B^\circ$ and Z. Finally, the semi-empirical correlation between these Ω_{stab} values and the two independent model parameters $\omega_B^\circ \cdot \sigma_B^\circ$ and Z is established, leading to the expression in the [ ] parenthesis of Eq. [30]. Now, let us explain the origin of the first, exponential term of Eq. [30]. For an average alloy, the T-dependence of its interaction energy is written as[118,119]:

$$\frac{\Omega_{0K}}{\Omega} \cong \exp\left(\frac{T}{3000}\right) \qquad [31]$$

Table II. Coordinates for the Data-Points Given in Figs. 6(a) to (c) for W–B Systems ($\omega_B^\circ \cdot \sigma_B^\circ$ and Ω are valid at $T = 0$ K, see Appendix A)

Component B	$\omega_B^\circ \cdot \sigma_B^\circ$ (kJ/mol)	Ω (kJ/mol)	Ng	NG Stability	Alloy Type
Ag	20.6	160	7.8	strong	3
Al	21.6	− 14	− 0.65	none	1
Ce	22.9	144	6.3	strong	3
Co	30.6	− 5	− 0.16	none	1
Cr	29.1	45	1.5	weak	3
Cu	22.7	200	8.8	strong	3
Fe	31.8	0	0	none	1
Mn	21.0	160	7.6	strong	3
Mo	43.1	− 1	− 0.02	none	1
Nb	43.0	− 33	− 0.77	none	1
Ni	30.1	− 12	− 0.42	none	1
Sc	26.9	44	1.6	weak	3
Ta	46.6	0	0	none	1
Ti	37.8	33	0.87	partial	2
W	49.8	—	—	—	—
Y	29.6	112	2.8	medium	3
Zr	40.9	− 36	− 0.88	none	1

The Ng numbers are calculated by Eq. [28]. Evaluation of NG stability: "none" for $Ng \leq 0.6$, "partial" for $Ng = 0.6 \ldots 1$, "weak" for $Ng = 1 \ldots 2$, "medium" for $Ng = 2 \ldots 4$ and "strong" for $Ng > 4$.

For an average value of $x = 0.15 \pm 0.05$, Eq. [29] leads to $Z \cong 0.022 \cdot T$ (where T is substituted in K, and Z is obtained in kJ/mol). Expressing T from this equation and substituting it into Eq. [31], the first exponential term of Eq. [30] is obtained, which is a correction factor for the T-dependence of the interaction energy. Note that ω_B° slightly increases, while σ_B° slightly decreases with temperature, and thus no correction is used in Eq. [30] for the T-dependence of $\omega_B^\circ \cdot \sigma_B^\circ$.

Now, let us find the conditions to form unstable (type 1) PC-NG alloys. This corresponds to the largest value of the interaction energy that is still with no minimum point in the molar Gibbs energy of the NG alloy as function of its grain size. Its approximated function is expressed by an equation, being similar to Eq. [30]:

$$\Omega_{\text{no-st}} \leq \exp\left(\frac{Z}{66}\right) \cdot [2.19 + 0.950 \cdot Z + \omega_B^\circ \cdot \sigma_B^\circ \cdot (0.518 + 0.00487 \cdot Z)] \quad [32]$$

where all physical quantities are substituted and obtained in kJ/mol. The parameters in the [ ] parenthesis of Eq. [32] are obtained similarly as above for Eq. [30]. The exponential term of Eq. [32] is the same as in Eq. [30], and is found using the same logic as above. Let us note that Eq. [32] at $Z = 0$ and in the characteristic range of $\omega_B^\circ \cdot \sigma_B^\circ = 20 \ldots 40$ kJ/mol can be written approximately as $Ng \cong 0.6$. Thus, the alloy types can be categorized at $T = 0$ K as:

1. if for a given A–B system $Ng \leq 0.6$, then this system is unstable as an NG alloy at any temperature and composition (*i.e.*, it is alloy type 1),
2. if for a given A–B system $0.6 < Ng \leq 1$, then this system is partly stable as an NG alloy (*i.e.*, it is alloy type 2), at least in a limited temperature and concentration range.
3. if for a given A–B system $Ng > 1$, then this system is fully stable as an NG alloy (*i.e.*, it is alloy type 3), at least in a limited temperature and concentration range.

Using the above principle, the 16 binary W-based systems in Table II are predicted as:

1. stable NG alloys are expected in the W-Cu, W-Ag, W-Mn, W-Ce, W-Y, W-Cr and W-Sc systems,
2. the W-Ti alloy is expected to be a partly stable NG alloy,
3. unstable NG alloys are expected to form in the W-Al, W-Co, W-Fe, W-Mo, W-Nb, W-Ni, W-Ta and W-Zr systems.

In Figures 6(a) through (c), the stability diagrams for NG alloys are shown at selected values of parameter Z, showing two demarcation lines calculated by Eqs. [30] and [32]. Those lines divide Figures 6(a) through (c) into the following 3 regions at any x–T, corresponding to the given Z:

i. the lower regions of Figures 6(a) through (c) correspond to systems of stable macroscopic alloys (= type 1 alloy);

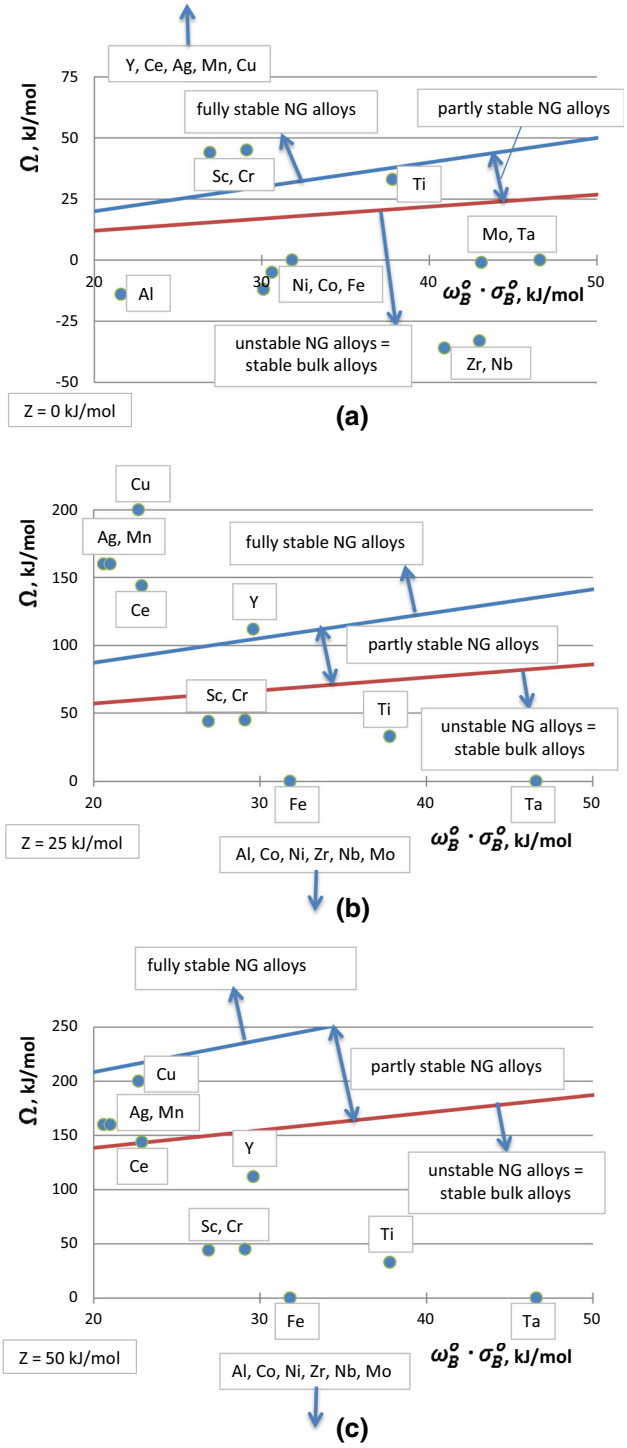

Fig. 6—The NG stability diagrams at $Z = 0$ (*a* at $T = 0$ K), at $Z = 25$ kJ/mol (*b*; at $x = 0.2$ it corresponds to $T = 1195$ K) and at $Z = 50$ kJ/mol (*c*; at $x = 0.2$ it corresponds to $T = 2391$ K) with 16 points of the 16 binary W-based systems. The straight lines are calculated by Eqs. [30] and [32]. Points are taken from Table II.

ii. the middle regions of Figure 6(a) through (c) correspond to systems of partly stable NG alloys (= type 2 alloys);

iii. the upper regions of Figures 6(a) through (c) correspond to systems of fully stable NG alloys (= type 3 alloys).

As follows from Figures 6(a) through (c), by increasing the value of Z (*i.e.*, increasing T at fixed x) the demarcation lines are shifted towards higher Ω values. Thus, increasing temperature type 3 alloys become first type 2 alloys and then type 1 alloys. This is due to the effect of entropy, stabilizing macro-solutions and destabilizing GB segregation as a 2-D ordered state.

IX. ON THE STABLE REGION OF NG ALLOYS IN THE W-AG PHASE DIAGRAM

As was shown above, in some A–B systems, the NG alloy is found fully stable in finite temperature and composition ranges. This theoretical prediction is of primary importance. However, the next reasonable question is about the theoretical prediction on the temperature and compositional borders of this stability range. The usual way to show the stability of different states in materials science is to present stable phases/states in equilibrium phase diagrams. For binary macroscopic systems phase diagrams are routinely constructed in T *vs* x diagrams at fixed $p = 1$ bar.[120] Thus, for engineering purposes the stability of NG alloys should be shown in the same type of phase diagrams. In this section an example will be shown for the W-Ag system, found stable till a relatively high temperature (see Table II and Figures 6(a) through (c)).

The collection of thermodynamic properties needed for the calculation of the extended W-Ag phase diagram is given in Table III. As follows from this table, W is considered as component A and Ag is considered as component B in the calculations, as the latter has a lower GB energy. The existing phase diagram is shown in Figure 7(a). This diagram is drawn by us, based on the information on negligible solubilities between bcc-W and fcc-Ag or bcc-W and liquid Ag at $p = 1$ bar.[120]

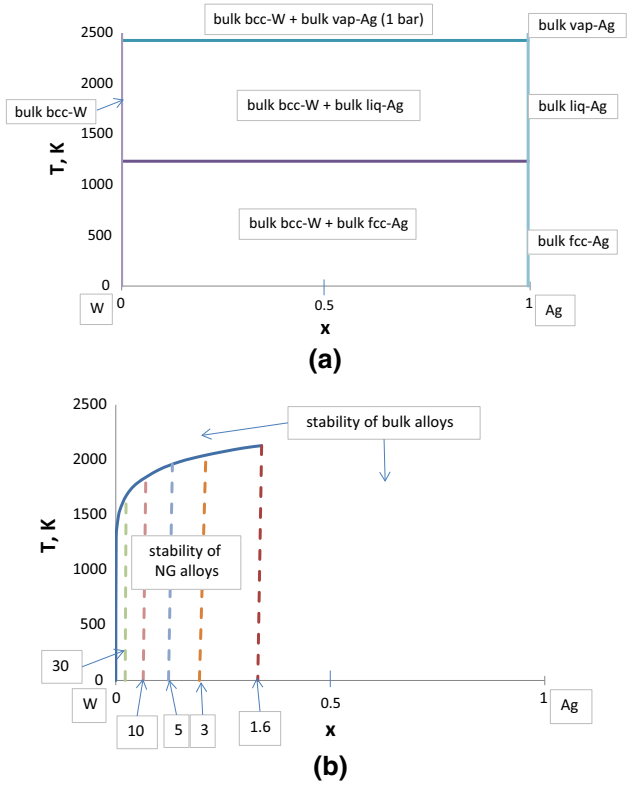

Fig. 7—The W-Ag equilibrium phase diagram. The current version from the literature (*a*) is drawn based on the information on almost no mutual miscibility of the components in macroscopic solid and liquid states. The region of stability of NG alloys in the W-rich corner of the phase diagram is shown in the (*b*). Almost vertical-dotted lines show iso-grain-radius lines in nm. The calculated stability region of the NG alloy is terminated at the Ag-rich side by the equilibrium grain radius of 1.6 nm.

Table III. Thermodynamic Properties of the W–Ag System (T in K)

Quantity	Unit	Equation	T-Range (K)	Source
$G^{\circ}_{m,W,bcc}$	J/mol	0	0 … 3695	121
$G^{\circ}_{m,Ag,bcc}$	J/mol	$3400 - 1.05 \cdot T$	0 … 3000	121
$G^{\circ}_{m,Ag,fcc}$	J/mol	0	0 … 1235	121
$G^{\circ}_{m,Ag,L}$	J/mol	$11508.141 - 9.301748 \cdot T$	1235 … 2433	121
$G^{\circ}_{m,Ag,V}$	J/mol	$292992 - 224.04 \cdot T + 12.686 \cdot T \cdot \ln T + R \cdot T \cdot \ln\left(\frac{p}{p^{\circ}}\right)$	$T \geq 2433$ K at $p = 1$ bar)	122
$V^{\circ}_{m,W}$	cm^3/mol	$9.47 \cdot \left(1 + 2.04 \cdot 10^{-5} \cdot T\right)$	0 … 3000	123, 124
$V^{\circ}_{m,Ag}$	cm^3/mol	$10.146 + 7.077 \cdot 10^{-5} \cdot T^{1.314}$	0 … 1235	125
		$9.889 + 8.694 \cdot 10^{-4} \cdot T$	1235 … 3000	
$V^{\circ}_{m,L,Ag}$	cm^3/mol	$10.490 + 9.648 \cdot 10^{-5} \cdot T^{1.314}$	0 … 1235	125
		$10.140 + 1.185 \cdot 10^{-3} \cdot T$	1235 … 3000	
σ°_{W}	J/m^2	$1.054 - 4.55 \cdot 10^{-5} \cdot T$	0 … 3000	Appendix A
σ°_{Ag}	J/m^2	$0.393 - 3.05 \cdot 10^{-5} \cdot T$	0 … 3000	Appendix A
Ω	kJ/mol	$160 \cdot \exp\left(-\frac{T}{4900}\right)$	0 … 3000	Appendix A

For the W-Ag system, the algorithm of calculation shown above should be slightly modified, as in this case the crystal structures of the two components are different.[121] Moreover, the NG stability is found also above the melting point of Ag. Thus, the reference molar Gibbs energies for macroscopic phases are calculated in different T-ranges as:

$$\text{at } T = 0 \ldots 1235\text{ K} : \text{bcc - W} + \text{fcc - Ag} : G_{\text{m,macro}} = 0 \quad [33a]$$

$$\text{at } 2433\text{ K} \geq T \geq 1235\text{ K} : \text{bcc - W} + \text{liq - Ag} : G_{\text{m,macro}} = x \cdot G^{\circ}_{\text{m,Ag,L}} \quad [33b]$$

$$\text{at } T \geq 2433\text{ K}(1\text{bar}) : \text{bcc - W} + \text{vap - Ag} : G_{\text{m,macro}} = xG^{\circ}_{\text{m,Ag,V}} \quad [33c]$$

where x (dimensionless) is the average mole fraction of Ag in the alloy. For the same reason, Eq. [26] should be modified with a new first term as:

$$G_{\text{m,nano,b}} = x_{\text{b}} \cdot G^{\circ}_{\text{m,Ag,bcc}} + R \cdot T \cdot [x_{\text{b}} \cdot \ln x_{\text{b}} + (1 - x_{\text{b}}) \cdot \ln(1 - x_{\text{b}})] + \Omega \cdot x_{\text{b}} \cdot (1 - x_{\text{b}}) \quad [34]$$

As the bulk of the grains are W-rich bcc-crystals, the molar grain boundary areas of both components are calculated using parameter $f = 1.25$ (see above). Let us note that in this case different molar volumes are used for solid and liquid Ag and also their T-dependencies are taken into account (see Table III).

The calculation procedure includes the construction of molar Gibbs energy diagrams similar to Figures 5(a) through (c) using different values of temperatures and average mole fractions of Ag. The first conclusion from each such diagram is whether at any grain size the molar Gibbs energy of the NG alloy calculated by Eqs. [22], [25], [27] and [34] is more negative than the most negative of the molar Gibbs energies of the corresponding macroscopic states calculated by Eqs. [33a] through [33c]. If the answer is "yes", then at the given T–x point of the W-Ag phase diagram the NG alloy is found stable. If the answer is "no", then at the given T–x point of the W-Ag phase diagram the original stable state shown in Figure 7(a) is found stable. In this way the contours of the full stability of the NG alloy can be drawn in the phase diagram, as shown in left bottom part of Figure 7(b).

Additionally, for the case of stable NG alloy, the equilibrium grain radius corresponding to the minimum of the molar Gibbs energy of the NG alloy can be found. Using these data, the iso-grain-radius lines were drawn as dotted, almost vertical lines in Figure 7(b). The stability range of the NG alloys is terminated when the equilibrium grain size reaches the smallest allowed value ($r = 1.6$ nm, see above), as at a higher Ag-content the equilibrium grain size would be smaller than this value and for such small grains the validity of the present model becomes questionable. Therefore, this line in Figure 7(b) is shown as a dotted line, as the choice of 1.6 nm above was somewhat arbitrary. The stability region of the NG alloy in the W-rich side of the phase diagram Figure 7(b) starts at $T = 0$ K at $x = 0$ and terminates at $x = 0.33 \ldots 0.34$ at $T = 0 \ldots 2130$ K.

It should be noted that the stability region of NG alloys in Figure 7(b) extends above the melting point of Ag. This might mean GB melting. However, in this model the GB is supposed to be amorphous / quasi-liquid anyway, and so this change is not reflected in Figure 7(b). However, it might have an influence on properties of the NG alloys.

Similar extended phase diagrams can be calculated for any other system with its Ng number being higher than 1. Such extended phase diagrams are considered useful tools for NG alloy design. Let us note that for all systems with the Ng number not exceeding 1 the existing macroscopic phase diagrams remain valid,[120] so for them the production of fully stable NG alloys (type 3) is hopeless.

X. CONCLUSIONS

1. It is shown that one-component poly-crystalline nano-grained (NG) metals are prone to grain coarsening due to their always positive GB energies.
2. Using the extended Butler equation, thermodynamic conditions are found for negative GB energy of binary nano-alloys (note: for macro-alloys only positive GB energies exist). This finding is built into a general thermodynamic model describing the molar Gibbs energy of NG alloys. Three types of alloys are considered: (i). the Type 1 NG alloy is unstable, as its molar Gibbs energy has no minimum as function of grain size, moreover, its molar Gibbs energy is more positive than that of the most stable macro-alloy ("unstable" here means it is not stable against grain coarsening and precipitation of a macro-phase); (ii). the Type 2 NG alloy is partly stable, as its molar Gibbs energy passes through a minimum as function of grain size, but its value is more positive than that of the most stable macro-alloy ("partly stable" here means it is stable against grain coarsening but not stable against precipitation of a macro-phase); (iii). the Type 3 NG alloy is fully stable, as its molar Gibbs energy passes through a minimum as function of grain size, and this molar Gibbs energy is more negative than that of the most stable macro-alloy ("fully stable" here means the NG alloys is stable both against grain coarsening and the precipitation of a macro-phase).
3. A new dimensionless number Ng is defined as the ratio of the bulk interaction energy between the A–B components to the molar excess GB energy of the solute component B at zero Kelvin. Based on the value of this Ng number all A–B systems can be categorized, at least at $T = 0$ K. When the Ng

number is smaller then 0.6, the A–B system is type 1. The A–B system is a type 2 alloy when the *Ng* number is between 0.6 and 1 and it is a type 3 alloy if the *Ng* number is larger than 1. Higher is the Ng number for the given A–B system, the wider is the temperature—composition space of the A–B alloy that is stable as an NG alloy. With increasing temperature systems gradually transform from type 3 to type 2 and further to type 1.

4. General equations are worked out for the critical values of the interaction energy as function of temperature, composition and excess molar GB energy of component B. These special interaction energy values serve as demarcation values/lines to separate alloys type 1 from alloys type 2 and those from alloys type 3. The method is demonstrated on 16 binary W-based alloys (see Table II and Figures 6(a) through (c)).
5. The temperature and concentration ranges of stability of NG alloys are calculated for the W-Ag system as an example, and the findings are presented in the binary equilibrium W-Ag phase diagram, indicating also iso-grain-size lines (see Figure 7(b)). The same method can be applied to calculate the stability ranges of other NG alloys with $Ng > 1$.

ACKNOWLEDGMENTS

Open access funding provided by University of Miskolc (ME). This work was partly financed by the ICARUS project which has received funding from the European Union's Horizon 2020 research and innovation program under Grant Agreement No 713514 and partly by the nano-Ginop Project GINOP-2.3.2-15-2016-00027 in the framework of the Szechenyi 2020 program, supported by the European Union. The author is grateful to the following individuals for their helpful discussions during this work: prof. Santiago Cuesta-López and prof. Nicolas A. Cordero of the University of Burgos (Spain), dr. Antonio Locci and prof. Francesco Delogu of the University of Calgary (Italy), Dr Tomas Polcar of Advamant Ltd (UK), prof. Antonio Rinaldi of ENEA (Italy), Andras Dezso, prof. Andras Roósz, prof. Zoltan Gacsi and dr. Greta Gergely of the University of Miskolc (Hungary), prof. Spiros Pantelakis of the University of Patras (Greece), prof Pal Barczy and Tamas Barczy of Admatis Ltd (Hungary). The author is also grateful for Anna Vasileva and Koppány Juhász for their help in the figures to this paper.

OPEN ACCESS

APPENDIX A: THE SOURCE OF DATA GIVEN IN TABLES II THROUGH III

The molar volumes of the elements are taken from References 123 through 125. The GB energies of pure elements are estimated from the surface tension of the same metal at their melting point as[100]:

$$\sigma^{\circ}_{\mathrm{Tm}} \cong \frac{1.15}{3} \cdot \sigma^{\circ}_{\mathrm{lg,Tm}} \qquad [A1]$$

where $\sigma^{\circ}_{\mathrm{Tm}}$ (J/m^2) is the GB energy at the melting point, $\sigma^{\circ}_{\mathrm{lg,Tm}}$ (J/m^2) is the surface tension of the same pure liquid metal at the melting point, coefficient 1.15 is the average ratio of surface energy of the solid to the surface tension of the liquid, while coefficient 1/3 is the ratio of GB energy to the surface energy. Eq. [A1] is valid for simple pure metals with their stable crystal structures of bcc, fcc or hcp. Further, the temperature dependence of the GB energies of pure metals is derived. For that, let us write a simplest model equation:

$$\sigma^{\circ} \cong \frac{\alpha \cdot H^{\circ}_{\mathrm{c,s}}}{f \cdot \left(V^{\circ}_{\mathrm{m,s}}\right)^{2/3} \cdot N_{\mathrm{Av}}^{1/3}} \qquad [A2]$$

where $H^{\circ}_{\mathrm{c,s}}$ (J/mol) is the cohesion energy within the pure solid metal, $V^{\circ}_{\mathrm{m,s}}$ (m^3/mol) is the molar volume of the pure solid metal, $N_{\mathrm{Av}} = 6.02 \cdot 10^{23}$ 1/mol is the Avogadro number, α and f (both dimensionless) are model parameters; they (or at least their ratio) are taken as constant for simple metals of bcc, fcc or hcp structures. For simplicity, the effect of excess interfacial entropy is neglected in Eq. [A2]. As only parameters $H^{\circ}_{\mathrm{c,s}}$ and $V^{\circ}_{\mathrm{m,s}}$ are T-dependent in Eq. [A2], the ratio of the GB energy of the same pure metal at $T = 298$ K and at its melting point can be written as:

$$\frac{\sigma^{\circ}_{298}}{\sigma^{\circ}_{\mathrm{Tm}}} \cong \frac{H^{\circ}_{\mathrm{c,s,298}}}{H^{\circ}_{\mathrm{c,s,Tm}}} \cdot \left(\frac{V^{\circ}_{\mathrm{m,s,Tm}}}{V^{\circ}_{\mathrm{m,s,298}}}\right)^{2/3} \qquad [A3]$$

Using the data for the molar volumes,[123–125] the GB energy can be estimated using Eq. [A3] as a linear function of temperature, through the two temperature values of 298 K and the melting point. The cohesion energies of solid metals are uncertain, as in thermodynamics the standard state is usually selected such that this quantity is eliminated (see Eq. [6]). That is why these quantities are estimated from the measured surface tension data and the model on the surface tension of pure liquid metals at their melting points (see Eq. [11] in Reference 115):

$$\sigma^{\circ}_{\mathrm{lg,Tm}} \cong \frac{(-0.174 \pm 0.023) \cdot H^{\circ}_{\mathrm{c,l,Tm}} + (1.2 \pm 2.3) \cdot T_{\mathrm{m}}}{(1.00 \pm 0.02) \cdot \left(V^{\circ}_{\mathrm{m,l,Tm}}\right)^{2/3} \cdot N_{\mathrm{Av}}^{1/3}} \quad [A4]$$

where $\sigma^{\circ}_{\mathrm{lg,Tm}}$ (J/m^2) is the surface tension of pure liquid metal at its melting point T_{m} (K), $H^{\circ}_{\mathrm{c,l,Tm}}$ (J/mol) is the cohesion energy of the pure liquid metal at its melting point, $V^{\circ}_{\mathrm{m,l,Tm}}$ (m^3/mol) is the molar volume of the pure liquid metal at its melting point, the numerical values of Eq. [A4] are theoretical values derived in Reference 115 for liquid metals resulting from fcc, hcp and bcc metals. Experimental data on the surface tensions of pure liquid metals at their melting points are taken from Reference 126. Using these values and Eq. [A4], the cohesion energy of pure liquid metals can be estimated at their melting points. From here, the cohesion enthalpy of the solid metal at its melting point is calculated as:

$$H^{\circ}_{\mathrm{c,s,Tm}} = H^{\circ}_{\mathrm{c,l,Tm}} - \Delta_{\mathrm{m}} H^{\circ} \quad [A5]$$

where $\Delta_{\mathrm{m}} H^{\circ}$ (J/mol) is the standard enthalpy of melting of a pure metal, given in Reference 122. The same is re-calculated to room temperature as:

$$H^{\circ}_{\mathrm{c,s,298K}} = H^{\circ}_{\mathrm{c,s,Tm}} - \int_{298}^{\mathrm{Tm}} C_{\mathrm{p}} \cdot \mathrm{d}T \quad [A6]$$

where C_{p} (J/molK) is the heat capacity of the pure solid metal defined at constant pressure of 1 bar; in Eq. [A6] the enthalpy changes due to solid phase transitions are also taken into account but not shown here. All these data are taken from Reference 122. The results of calculations are given in Tables II through III.

It should be noted that many compilations exist for surface energies of solid metals (see for example Reference 127) and for grain boundaries (see for example References 128 through 130). However, experimental uncertainties in measuring any interfacial energy involving any solid phase is much higher compared to the experimental uncertainty of measured surface tension of liquids. This also follows from Reference 129, where the high uncertainty of grain boundary energies is shown from different sources. To make sure the GB energy values used in this paper are coherent within each other, our model was started from the reliable data on surface tension. Nevertheless, our data in Tables II through III are not in contradiction with measured values.[127–130]

The interaction energies for the binary systems are taken from measured enthalpies of mixing[131,132] and from Calpad assessments.[133–150] The data from the Miedema model[151] were also taken into account, but not preferred. In absence of Calphad-type assessments the interaction energies were estimated from the phase diagrams.[120] For phase diagrams with solid or liquid miscibility gap with known (or estimated) critical temperature, the interaction energy is estimated as:

$$\Omega \cong 2 \cdot R \cdot T_{\mathrm{cr}} \quad [A7]$$

where T_{cr} (K) is the critical (maximum) point of the miscibility gap. The same Eq. [A7] is used when the fact of immiscibility is established in the given system, but no further details are known. Then, instead of T_{cr} the melting point of the higher-melting point component is taken, and in this case only the possible minimum value of Ω can be calculated. For phase diagrams with liquid miscibility gap with known monotectic temperature (T_{mon}, K) and known mole fraction of the high-melting point component (x), the interaction energy is estimated as:

$$\Omega \cong R \cdot T_{\mathrm{mon}} \cdot \ln(x/1-x)/2x - 1 \quad [A8]$$

For phase diagram with known eutectic temperature (T_{eu}, K) and known eutectic mole fraction (x) of the higher-melting point component, the interaction energy is estimated as:

$$\Omega \cong \frac{G^{\circ}_{\mathrm{M,s}} - G^{\circ}_{\mathrm{M,l}} - R \cdot T_{\mathrm{eu}} \cdot \ln x}{(1-x)^2} \quad [A9]$$

where $G^{\circ}_{\mathrm{M,s}}$ (J/mol) is the standard Gibbs energy of the solid higher-melting point metal,[121] $G^{\circ}_{\mathrm{M,l}}$ (J/mol) is the standard Gibbs energy of the liquid higher-melting point metal.[121] These estimated values are always obtained at the given temperature (T_{cr}, T_{mon}, T_{eu}). Their T-dependence is expressed as follows[111,119,152]:

$$\Omega = \Omega_{0\mathrm{K}} \cdot \exp\left(-\frac{T}{\tau}\right) \quad [A10]$$

$$\tau \cong T_{\mathrm{m,A}} + T_{\mathrm{m,B}} \quad [A11]$$

where $\Omega_{0\mathrm{K}}$ (J/mol) is the interaction energy at $T = 0$ K, τ (K) is found approximately using the data of Reference 121.

NOMENCLATURE

A	The total interface area of grain boundaries (m^2)
A_{sp}	The average specific interfacial area of the grain boundaries (1/m)
f	A geometric parameter in Eqs. [8a] through [8b] ($\cong$ 1.25 for bcc grain) (–)
f_{b}	The bulk packing fraction within the grain (= 0.68 for bcc grain (–)
f_{gb}	The 2-dimensional packing fraction along the GB (= 0.75) (–)
G°_{A}	The Gibbs energy of pure component A with GBs (J)
$G^{\circ}_{\mathrm{b,A}}$	The bulk Gibbs energy of pure component A without GBs (J)
$G^{\circ}_{\mathrm{m,A}}$	The molar Gibbs energy of pure component A with GBs (J/mol)
$G^{\circ}_{\mathrm{m,b,A}}$	The molar Gibbs energy of pure component A without GBs (J/mol)
$G^{\circ}_{\mathrm{m,Ag,L}}$	The standard molar Gibbs energy of pure silver in liquid state (J/mol)

$G^{\circ}_{m,Ag,V}$	The standard molar Gibbs energy of pure silver in vapor state (J/mol)
$G^{\circ}_{m,b,B}$	The molar Gibbs energy of pure component B without GBs (J/mol)
$G_{m,mac}$	The molar Gibbs energy of equilibrium mixture of two macroscopic solid solutions (J/mol)
$G_{m,nano}$	The molar Gibbs energy of the NG alloy (J/mol)
$G_{m,nano,b}$	The bulk molar Gibbs energy of the NG alloy (J/mol)
k	A semi-empirical constant of Eq. [4], ($k \cong 3.36$) (–)
n°_{A}	The amount of matter in the pure phase A (mole)
n_b	The amount of matter within the bulk of one average grain (mole)
n_{gb}	The amount of matter in the half-GB (mole)
$n_{B,gb}$	The amount of matter of component B in the half-GB (mole)
N_{Av}	The Avogadro number ($= 6.02 \times 10^{23}$) (1/mole)
Ng	The dimensionless Ng-number defined by Eq. [28] (–)
p	Pressure in the system (Pa)
r	The average effective grain radius (for a spherical grain) (m)
r_a	The atomic radius (m)
r_{min}	The minimum size of the grain hat ensures the GB is fully covered by component B (m)
R	The universal gas constant ($= 8.3145$ J/molK)
T	Absolute temperature (K)
V	The total volume of the NG metal (m^3)
V_b	The volume of the bulk of one average grain (m^3)
$V_{m,b}$	The molar volume of the bulk of the grain (m^3/mol)
$V^{\circ}_{m,A}$	The molar volume of pure component A (m^3/mol)
$V^{\circ}_{m,B}$	The molar volume of pure component B (m^3/mol)
$V^{\circ}_{m,L,B}$	The molar volume of pure liquid component B (m^3/mol)
Z	The dimensionless number defined by Eq. [29] (–)
x	The average mole fraction of component B in the alloy (–)
x_b	The mole fraction of component B in the bulk of the grain (–)
x_{gb}	The mole fraction of component B in the GB (–)
x_e	x_e and $1 - x_e$ are the equilibrium mole fractions of B in case of phase separation of bulk alloy A–B (–)
x_{min}	The minimum average mole fraction of component B, needed to stabilize the grain (–)
A	The first component (subscript) (–)
a	Atomic (subscript) (–)
b	Bulk (subscript) (–)
B	The second component (subscript) (–)
L	Liquid (subscript) (–)
m	Molar (subscript) (–)
mac	Macroscopic (subscript) (–)
min	Minimum (subscript) (–)
nano	Nanosized (–)
NG	Poly-crystalline nano-grained alloy (–)
no-st	No-stability (subscript) (–)
stab	Stability (subscript) (–)
β	The ratio of bonds in the GB to the same in the bulk of the grain (–)
σ	The grain boundary energy of alloy A–B (J/m^2)
σ_A	The partial grain boundary energy of component A in alloy A–B (J/m^2)
σ°_{A}	The grain boundary (free) energy in a pure A crystal (J/m^2)
σ_B	The partial grain boundary energy of component B in alloy A–B (J/m^2)
σ°_{B}	The grain boundary (free) energy in a pure B crystal (J/m^2)
ω°_{A}	The molar GB interfacial area in pure crystal A (m^2/mol)
ω°_{B}	The molar GB interfacial area in pure crystal B (m^2/mol)
Ω	The bulk interaction energy between components A and B (J/mol)
Ω_{gb}	The special Ω value ensuring $\sigma = 0$ (J/mol)
Ω_{cr}	The critical Ω value above which phase separation takes place (J/mol)
Ω_{stab}	The minimum interaction energy needed to fully stabilize the NG alloy (J/mol)
Ω_{no-st}	The largest value of the interaction energy below which there is even no partial stability of the NG alloy (J/mol)

REFERENCES

1. A. Táborosi, R.K. Szilagyi, B. Zsirka, O. Fónagy, E. Horváth, and J. Kristóf: *Inorg. Chem.*, 2018, vol. 57, pp. 7151–67.
2. E. Illés, M. Szekeres, I.Y. Tóth, Á. Szabó, B. Iván, R. Turcu, L. Vékás, I. Zupkó, G. Jaics, and E. Tombácz: *J. Magn. Magn. Mater.*, 2018, vol. 451, pp. 710–20.
3. K. Molnar, C. Voniatis, D. Feher, A. Ferencz, G. Weber, M. Zrinyi, and A. Jedlovszky-Hajdu: *Byophys. J.*, 2018, vol. 114, p. 363a.
4. Z. Fogarassy, N. Oláh, I. Cora, Z.E. Horváth, T. Csanádi, A. Sulyok, and K. Balázsi: *J. Eur. Ceram. Soc.*, 2018, vol. 38, pp. 2886–92.
5. M. Weszl, K.L. Tóth, I. Kientzl, P. Nagy, D. Pammer, L. Pelyhe, N.E. Vrana, D. Scharnweber, C. Wolf-Brandstetter, J.F. Árpád, and E. Bognár: *Mater. Sci. Eng. C*, 2018, vol. 78, pp. 69–78.
6. É. Fazakas, Z. Mátyás-Karácsony, R. Bak, and L.K. Varga: *Am. J. Anal. Chem.*, 2017, vol. 8, pp. 171–79.
7. G.F. Samu, Á. Veres, S.P. Tallósy, L. Janovák, I. Dékány, A. Yepez, R. Luque, and C. Janáky: *Catal. Today*, 2017, vol. 284, pp. 3–10.
8. M. Czagány, P. Baumli, and G. Kaptay: *Appl. Surf. Sci.*, 2017, vol. 423, pp. 160–69.
9. O. Pitkänen, T. Järvinen, H. Cheng, G.S. Lorite, A. Dombovari, L. Rieppo, S. Talapatra, H.M. Duong, G. Tóth, K.L. Juhász, Z. Kónya, A. Kukovecz, P.M. Ajayan, R. Vajtai, and K. Kordás: *Sci Rep.*, 2017, vol. 7, p. 16594.
10. F. Bíró, C. Dücső, G.Z. Radnóczi, Z. Baji, M. Takács, and I. Bársony: *Sens. Actuators B*, 2017, vol. 247, pp. 617–25.

11. V. Takáts, J. Hakl, A. Csík, H.F. Bereczki, G. Lévai, M. Godzsák, T.I. Török, G. Kaptay, and K. Vad: *Surf. Coat. Technol.*, 2017, vol. 326, pp. 121–25.
12. O. Tapasztó, J. Balko, V. Puchy, P. Kun, G. Dobrik, Z. Fogarassy, Z.E. Horváth, J. Dusza, K. Balázsi, C. Balázsi, and L. Tapasztó: *Sci Rep.*, 2017, vol. 7, p. 10087.
13. W. Rao, D. Wang, T. Kups, E. Baradács, B. Parditka, Z. Erdélyi, P. Schaaf, and A.C.S. Appl: *Mater. Interfaces*, 2017, vol. 9, pp. 6273–81.
14. G. Czel, K. Tomolya, M. Sveda, A. Sycheva, F. Kristaly, A. Roosz, and D. Janovszky: *J. Non-Cryst. Solids*, 2017, vol. 458, pp. 41–51.
15. N. Oláh, Zs. Fogarassy, A. Sulyok, M. Veres, G. Kaptay, and K. Balázsi: *Surf. Coat. Technol.*, 2016, vol. 302, pp. 410–19.
16. G. Levai, M. Godzsák, T.I. Török, J. Hakl, V. Takáts, A. Csik, K. Vad, and G. Kaptay: *Metall. Mater. Trans. A*, 2016, vol. 47A, pp. 3580–96.
17. A. Lekatou, A.E. Karantzalis, A. Evangelou, V. Gousia, G. Kaptay, Z. Gacsi, P. Baumli, and A. Simon: *Mater. Design*, 2015, vol. 65, pp. 1121–35.
18. O.L. Galkina, A. Sycheva, A. Blagodatskiy, G. Kaptay, V.L. Katanaev, G.A. Seisenbaeva, V.G. Kessler, and A.V. Agafonov: *Surf. Coat. Technol.*, 2014, vol. 253, pp. 171–79.
19. E. Sohn, X. Li, W.Y. He, S. Jiang, Z. Wang, K. Kang, J.H. Park, H. Berger, L. Forró, K.T. Law, J. Shan, and K.F. Mak: *Nat. Mater.*, 2018, vol. 17, pp. 504–08.
20. H. Gleiter: *Acta Mater.*, 2000, vol. 48, pp. 1–29.
21. R. Valiev: *Nat. Mater.*, 2004, vol. 3, pp. 511–16.
22. M.A. Meyers, A. Mishra, and D.J. Benson: *Prog. Mater. Sci.*, 2006, vol. 51, pp. 427–556.
23. M. Dao, L. Lu, R.J. Asaro, J.T.M. De Hosson, and E. Ma: *Acta Mater.*, 2007, vol. 55, pp. 4041–65.
24. R.H.R. Castro: *Mater Lett.*, 2013, vol. 96, pp. 45–56.
25. K. Lu: *Nat. Rev. Mater.*, 2016, vol. 1, p. 16019.
26. R.H.R. Castro and D. Gouvea: *J. Am. Ceram. Soc.*, 2016, vol. 99, pp. 1105–21.
27. T.J. Rupert: *Curr. Opin. Solid State Mater. Sci.*, 2016, vol. 20, pp. 257–67.
28. I.A. Ovidko, R.Z. Valiev, and Y.T. Zhu: *Prog. Mater. Sci.*, 2018, vol. 94, pp. 462–540.
29. P.K. Sahoo, S.S.K. Kamal, M. Premkumar, B. Sreedhar, S.K. Srivastava, and L. Durai: *Int. J. Refract. Met. Hard. Mater.*, 2011, vol. 29, pp. 547–54.
30. G.T.P. Azar, H.R. Rezaie, B. Gogari, and H. Razavizadeh: *J. Alloys Compds.*, 2013, vol. 574, pp. 432–36.
31. C. Ren, M. Koopman, Z.Z. Fang, H. Zhang, and B. van Devener: *Int. J. Refract. Met. Hard. Mater.*, 2016, vol. 61, pp. 273–78.
32. W.T. Qiu, Y. Pang, Z. Xiao, and Z. Li: *Int. J. Refract. Met. Hard. Mater.*, 2016, vol. 61, pp. 91–97.
33. C. Ren, Z.Z. Fang, H. Zhang, and M. Koopman: *Int. J. Refract. Met. Hard. Mater.*, 2016, vol. 61, pp. 273–78.
34. M. Kapoor, T. Kaub, K.A. Darling, B.L. Boyce, and G.B. Thompson: *Acta Mater.*, 2017, vol. 126, pp. 564–75.
35. J.T. Zhao, J.Y. Zhang, L.F. Cao, Y.Q. Wang, P. Zhang, K. Wu, G. Liu, and J. Sun: *Acta Mater.*, 2017, vol. 132, pp. 550–64.
36. Z.L. Zhang, J.M. Guo, G. Dehm, and R. Pippan: *Acta Mater.*, 2017, vol. 138, pp. 42–51.
37. S. Chakraverty, K. Sikdarm, S.S. Singh, D. Roy, and C.C. Koch: *J. Alloys Compds.*, 2017, vol. 716, pp. 197–203.
38. G. Csiszár, A. Makvandi, and E.J. Mittemeijer: *J. Appl. Cryst.*, 2017, vol. 50, pp. 152–71.
39. R. Raghavan, T.P. Harzer, S. Djaziri, S.W. Hieke, C. Kirchlechner, and G. Dehm: *J. Mater. Sci.*, 2017, vol. 52, pp. 913–20.
40. S.S.V. Tatiparti and F. Ebrahimi: *J. Alloys Compds.*, 2017, vol. 694, pp. 632–35.
41. P.S. Roodposthi, M. Saber, C. Koch, R. Scattergood, and S. Shahbazmohamadi: *J. Alloys Compds.*, 2017, vol. 720, pp. 510–20.
42. O.K. Donaldson, K. Hattar, T. Kaub, and G.B. Thomson: *J. Mater. Res.*, 2018, vol. 33, pp. 68–80.
43. J. Hu, Y.N. Shi, and K. Lu: *Scr. Mater.*, 2018, vol. 154, pp. 182–85.
44. H. Kotan: *J. Alloys Compds.*, 2018, vol. 749, pp. 948–54.
45. X.G. Li, L.F. Cao, J.Y. Zhang, J. Li, J.T. Zhao, X.B. Feng, Y.Q. Wang, K. Wu, P. Zhang, G. Liu, and J. Sun: *Acta Mater.*, 2018, vol. 151, pp. 87–99.
46. J.F. Curry, T.F. Babuska, T.A. Furnish *et al.*: *Adv. Mater.*, 2018, vol. 30, p. 1802026.
47. Y.Z. Chen, K. Wang, G.B. Shan, A.V. Ceguerra, L.K. Huang, H. Dong, L.F. Cao, S.P. Ringer, and F. Liu: *Acta Mater.*, 2018, vol. 158, pp. 340–53.
48. J. Weissmuller: *Nanostruct. Mater.*, 1993, vol. 3, pp. 261–72.
49. J. Weissmuller: *J. Mater. Res.*, 1994, vol. 9, pp. 4–7.
50. D.L. Beke, C. Cserháti, and I.A. Szabó: *Nanostr. Mater.*, 1997, vol. 9, pp. 665–68.
51. R. Kirchheim: *Acta Mater.*, 2002, vol. 40, pp. 413–19.
52. D.L. Beke, C. Cserháti, and I.A. Szabó: *J. Appl. Phys.*, 2004, vol. 95, pp. 4996–5001.
53. F. Liu and R. Kirchheim: *J. Cryst. Growth*, 2004, vol. 264, pp. 385–91.
54. F. Liu and R. Kirchheim: *Scripta Mater.*, 2004, vol. 51, pp. 521–25.
55. P.C. Millett, R.P. Selvam, S. Bansal, and A. Saxena: *Acta Mater.*, 2005, vol. 53, pp. 3671–78.
56. L.S. Shvindlerman and G. Gottstein: *Scripta Mater.*, 2006, vol. 54, pp. 1041–45.
57. R. Kirchheim: *Scripta Mater.*, 2006, vol. 55, pp. 963–64.
58. R. Kirchheim: *Acta Mater.*, 2007, vol. 55, pp. 5129–38.
59. R. Kirchheim: *Acta Mater.*, 2007, vol. 55, pp. 5139–48.
60. P.C. Millett, R.P. Selvam, and A. Saxena: *Acta Mater.*, 2007, vol. 55, pp. 2329–36.
61. J.R. Trelewicz and C.A. Schuh: *Phys. Rev B*, 2009, vol. 79, p. 094112.
62. F. Liu, Z. Chen, W. Yang, C.L. Yang, H.F. Wang, and G.C. Yang: *Mater. Sci. Eng. A*, 2010, vol. 457, pp. 13–17.
63. Y. Purohit, L. Sun, D.L. Irving, R.O. Scattergood, and D.W. Brenner: *Mater. Sci. Eng. A*, 2010, vol. 527, pp. 1769–75.
64. K.A. Darling, M.A. Tschopp, B.K. VanLeeuwen, M.A. Atwater, and Z.K. Liu: *Comput. Mater. Sci.*, 2014, vol. 84, pp. 255–66.
65. N.X. Zhou and J. Luo: *Mater. Lett.*, 2014, vol. 115, pp. 268–71.
66. T. Chookajorn, H.A. Murdoch, and C.A. Schuh: *Science*, 2012, vol. 337, pp. 951–54.
67. H.A. Murdoch and C.A. Schuh: *Acta Mater.*, 2013, vol. 61, pp. 2121–32.
68. H.A. Murdoch and C.A. Schuh: *J. Mater. Res.*, 2013, vol. 28, pp. 2154–63.
69. M. Saber, H. Kotan, C.C. Koch, and R.O. Scattergood: *J. Appl. Phys.*, 2013, vol. 113, p. 063515.
70. T. Chookajorn and C.A. Schuh: *Phys. Rev. B*, 2014, vol. 89, p. 064102.
71. T. Chookajorn and C.A. Schuh: *Acta Mater.*, 2014, vol. 73, pp. 128–38.
72. A.R. Kalidindi, T. Chookajoorn, and C.A. Schuh: *JOM*, 2015, vol. 67, pp. 2834–43.
73. F. Abdeljawad and S.M. Foiles: *Acta Mater.*, 2015, vol. 101, pp. 159–71.
74. N. Zhou, T. Hu, J. Huang, and J. Luo: *Scr. Mater.*, 2016, vol. 124, pp. 160–63.
75. T. Liang, Z. Chen, X. Yang, J. Zhang, and P. Zhang: *Int. J. Mater. Res.*, 2017, vol. 108, pp. 435–40.
76. O. Waseda, H. Goldenstein, G.F.B. Lenz Silva, A. Neiva, P. Chantrenne, J. Morthomas, M. Perez, C.S. Becquart, and R.G.A. Veiga: *Model. Simul. Mater. Sci. Eng.*, 2017, vol. 25, p. 075005.
77. D.A. Aksyonov and A.G. Lipnitskii: *Comput. Mater. Sci.*, 2017, vol. 137, pp. 266–72.
78. F. Abdeljawad, P. Lu, N. Argibay, B.G. Clarke, B.L. Boyce, and S.M. Foiles: *Acta Mater.*, 2017, vol. 126, pp. 528–39.
79. A.R. Kalidindi and C.A. Schuh: *Acta Mater.*, 2017, vol. 132, pp. 128–37.
80. Y. Zhang, G.J. Tucker, and J.R. Trelevicz: *Acta Mater.*, 2017, vol. 131, pp. 39–47.
81. A.R. Kalidindi and C.A. Schuh: *J. Mater. Res.*, 2017, vol. 32, pp. 1993–2000.
82. J.D. Schuler and T.J. Rupert: *Acta Mater.*, 2017, vol. 140, pp. 196–205.
83. S.B. Kadambi and S. Patala: *Phys. Rev. Mater.*, 2017, vol. 1, p. 043604.

84. F.D. Fischer, G.A. Zickler, and J. Svoboda: *Phil. Mag*., 2017, vol. 97, pp. 1963–77.
85. W.T. Xing, A.R. Kalidindi, and C.A. Schuh: *Scr. Mater*., 2017, vol. 127, pp. 136–40.
86. Y.J. Zhao and J.Q. Zhou: *J. Nanopart. Res*., 2017, vol. 19, p. 406.
87. C.J.O. Brien, C.M. Barr, P.M. Price, K. Hattar, and S.M. Foiles: *J. Mater. Sci*., 2018, vol. 53, pp. 2911–27.
88. K. Graetz, J.S. Paras, and C.A. Schuh: *Materialia*, 2018, vol. 1, pp. 89–98.
89. M.A. Tschopp, H.A. Murdoch, L.J. Kecskes, and K.A. Darling: *JOM*, 2014, vol. 66, pp. 1000–19.
90. R.A. Andrievski: *J. Mater. Sci*., 2014, vol. 49, pp. 1449–60.
91. M. Saber, C.C. Koch, and R.O. Scattergood: *Mater. Res. Lett*., 2015, vol. 3, pp. 65–75.
92. H.R. Peng, M.M. Gong, Y.Z. Chen, and F. Liu: *Int. Mater. Rev*., 2017, vol. 62, pp. 303–33.
93. P. Lejcek, M. Vsianska, and M. Sob: *J. Mater. Res*., 2018, vol. 33, pp. 2647–60.
94. G. Kaptay: *J. Mater. Sci*., 2012, vol. 47, pp. 8320–35.
95. G. Kaptay: *Adv. Colloid Interface Sci*., 2018, vol. 256, pp. 163–92.
96. J.W. Gibbs: Trans. Conn. Acad. Arts Sci. 1875–1878, vol. 3, pp. 108–248 and 343–524.
97. I. Langmuir: *J. Am. Chem. Soc*., 1918, vol. 40, pp. 1361–403.
98. D. McLean: *Grain Boundaries in Metals*, Clarendon Press, Oxford, 1957.
99. P. Lejcek: *Grain Boundary Segregation in Metals. Springer Series Maters Sci*, Springer, Berlin, 2010, vol. 136.
100. G. Kaptay: *J. Mater. Sci*., 2016, vol. 51, pp. 1738–55.
101. J.A.V. Butler: *Proc. R. Soc. A*, 1932, vol. 135, pp. 348–75.
102. C.C. Koch, R.O. Scattergood, K.A. Darling, and J.E. Semones: *J. Mater. Sci*., 2008, vol. 43, pp. 7264–72.
103. C.C. Koch, R.O. Scattergood, M. Saber, and H. Kotan: *J. Mater. Res*., 2013, vol. 28, pp. 1785–91.
104. B.G. Clark, K. Hattar, M.T. Marshall, T. Chookajorn, B.L. Boyce, and C.A. Schuh: *JOM*, 2016, vol. 68, pp. 1625–33.
105. D. Amram and C.A. Schuh: *Acta Mater*., 2018, vol. 144, pp. 447–58.
106. H.R. Peng, L.K. Huang, and F. Liu: *Mater. Lett*., 2018, vol. 219, pp. 276–79.
107. F.D. Fischer, J. Svoboda, and P. Fratzl: *Phil. Mag*., 2003, vol. 83, pp. 1075–93.
108. J. Li, J. Wang, and G. Yang: *Scr. Mater*., 2009, vol. 60, pp. 945–48.
109. M.M. Gong, F. Liu, and K. Zhang: *Scr. Mater*., 2010, vol. 63, pp. 989–92.
110. Z. Chen, F. Liu, X.Q. Yang, C.J. Shen, and Y.M. Zhao: *J. Alloys Compd*., 2014, vol. 608, pp. 338–42.
111. D.L. Beke, Yu. Kaganovskii, and G.L. Katona: *Progress Mater. Sci*., 2018, vol. 98, pp. 625–674.
112. G. Kaptay: *Langmuir*, 2015, vol. 31, pp. 5796–804.
113. J. Korozs and G. Kaptay: *Colloid Surf. A*, 2017, vol. 433, pp. 296–301.
114. A.S. Skapski: *J. Chem. Phys*., 1948, vol. 16, pp. 389–93.
115. G. Kaptay: *Mater. Sci. Eng. A*, 2008, vol. 495, pp. 19–26.
116. G. Kaptay: *Langmuir*, 2017, vol. 33, pp. 10550–560.
117. G. Kaptay: *Int. J. Pharm*., 2012, vol. 430, pp. 253–57.
118. G. Kaptay: *Calphad*, 2004, vol. 28, pp. 115–24.
119. G. Kaptay: *Calphad*, 2017, vol. 56, pp. 169–84.
120. T.B. Massalski, ed.: *Binary Alloy Phase Diagrams*, second ed., vol. 3, ASM International, New York, 1990.
121. A.T. Dinsdale: *Calphad*, 1991, vol. 15, pp. 317–425.
122. I. Barin: *Thermochemical Properties of Pure Substances*, VCh, 1993, in 2 parts.
123. J. Emsley: *The Elements*, Clarendon Press, Oxford, 1989.
124. Y.S. Touloukian, R.K. Kirby, R.E. Taylor, and T.Y.R. Lee: *Thermal Expansion*, IFI/Plenum, New York, 1977.
125. G. Kaptay: *J. Mater. Sci*., 2015, vol. 50, pp. 678–87.
126. T. Iida and R.I.L. Guthrie: *The Physical Properties of Liquid Metals*, Clarendon Press, Oxford, 1993.
127. G. Guisbiers, M. Jose-Yacaman: in *Reference Module in Chemistry, Molecular Sciences and Chemical Engineering*, Elsevier, Amsterdam, 2017.
128. D. Schreiber, V.I. Razumovskiy, P. Rusching, R. Pippan, and L. Romaner: *Acta Mater*., 2015, vol. 88, pp. 180–89.
129. D. Schreiber, R. Pippan, P. Ruschnig, and L. Romaner: *Model. Simul. Mater. Sci. Eng*., 2016, vol. 24, p. 035013.
130. D. Schreiber, R. Pippan, P. Ruschnig, and L. Romaner: *Model. Simul. Mater. Sci. Eng*., 2016, vol. 24, p. 085009.
131. B. Predel: *Phase Equilibria, Crystallographic and Thermodynamic Data of Binary Alloys, vol. 5 of group IV of Landolt-Börnstein Handbook*, Springer, Berlin, 1991–1997.
132. S.V. Meschel and O.J. Kleppa: *J. Alloys Compds*., 1993, vol. 197, pp. 75–81.
133. L. Kaufman and H. Nesor: *Calphad*, 1978, vol. 2, pp. 55–80.
134. L. Kaufman and H. Nesor: *Calphad*, 1978, vol. 2, pp. 80–108.
135. J.L. Murray: *Bull. Alloy Phase Diagr*., 1981, vol. 2, pp. 192–196.
136. J.O. Andersson and P. Gustaffson: *Calphad*, 1983, vol. 7, pp. 317–26.
137. S.K. Lee and D.N. Lee: *Calphad*, 1986, vol. 10, pp. 61–76.
138. P. Gustaffson: *Metall. Mater. Trans. A*, 1988, vol. 19A, pp. 2531–46.
139. M. Vijayakumar, A.M. Siriamamutry, and S.V.N. Naidi: *Calphad*, 1988, vol. 12, pp. 177–84.
140. K. Frisk and P. Gustaffson: *Calphad*, 1989, vol. 12, pp. 247–54.
141. L. Kaufman: *Calphad*, 1991, vol. 15, pp. 243–59.
142. N. Dupin and B. Sundman: *Metallurgy*, 2001, vol. 30, pp. 184–92.
143. L. Kaufman, P.E.A. Turchi, W. Huang, and Z.K. Liu: *Calphad*, 2001, vol. 25, pp. 419–33.
144. P.E.A. Turchi, V. Drchal, J. Kudrnovsky, C. Colinet, L. Kaufman, and Z.K. Liu: *Phys. Rev. B*, 2005, vol. 71, p. 094206.
145. J. Popovic, P. Broz, and J. Bursik: *Intermetallics*, 2008, vol. 16, pp. 884–88.
146. Y.F. Cui, X. Zhang, G.L. Xu, W.J. Zhu, H.S. Liu, and Z.P. Jun: *J. Mater. Sci*., 2011, vol. 46, pp. 2611–21.
147. S.Y. Yang, M. Jiang, H.X. Li, and L. Wang: *Trans. Nonferr. Met. Soc. China*, 2011, vol. 21, pp. 2270–75.
148. P. Zhou, Y. Peng, Y. Du, S. Wang, and G. Wen: *Int. J. Refract. Met. Hard. Mater*., 2015, vol. 50, pp. 274–81.
149. S.L. Wang, L.J. Zhou, Y. Ye, X.H. Wang, Y.H. Lin, C.P. Wang, and X.J. Liu: *J. Phase Equilib. Differ*., 2015, vol. 36, pp. 3–9.
150. H.W. Yao, J.W. Qiao, M.C. Gao, J.A. Hawk, S.G. Ma, H.F. Zhou, and Y. Zhang: *Mater. Sci. Eng. A*, 2016, vol. 674, pp. 203–11.
151. F.R. de Boer, R. Boom, W.C.M. Mattens, A.R. Miedema: *Cohesion in Metals*, North-Holland, Amsterdam, 1988.
152. G. Kaptay: *Metall. Mater. Trans. A*, 2012, vol. 43A, pp. 531–43.